Bacterial cell cycle regulator MatP forms biomolecular condensates and directly interacts with cell division protein FtsZ

Inés Barros-Medina[1†], Miguel Ángel Robles-Ramos[1†], Marta Sobrinos-Sanguino[1,2†], Juan Román Luque-Ortega[2], Carlos Alfonso[1], William Margolin[3], Germán Rivas[1], Begoña Monterroso[4*], Silvia Zorrilla[1*]

[1] Department of Cellular and Molecular Biosciences, Centro de Investigaciones Biológicas Margarita Salas, Consejo Superior de Investigaciones Científicas (CSIC). 28040 Madrid, Spain
[2] Molecular Interactions Facility, Centro de Investigaciones Biológicas Margarita Salas, Consejo Superior de Investigaciones Científicas (CSIC). 28040 Madrid, Spain
[3] Department of Microbiology and Molecular Genetics, McGovern Medical School, UTHealth-Houston, Houston, TX 77030, USA
[4] Department of Crystallography and Structural Biology, Instituto de Química Física Blas Cabrera, Consejo Superior de Investigaciones Científicas (CSIC). 28006 Madrid, Spain

† Joint First Authors, in alphabetical order

* Joint Last Authors, in alphabetical order; to whom correspondence should be addressed. BM: Tel: +34 91 561 94 00; Fax: +34 91 564 24 31; Email: bmonterroso@iqf.csic.es. SZ: Tel: +34 91 837 31 12; Fax; +34 91 536 04 32. Email: silvia@cib.csic.es.

ABSTRACT

Bacterial cytokinesis is driven by a contractile ring of FtsZ protein polymers at midcell. FtsZ can also form phase-separated biomolecular condensates with potential implications for cytokinesis and development of antibiotic-tolerant persister cells. In *Escherichia coli*, FtsZ ring positioning depends in part on the MatP protein, which binds DNA sites (*matS*) in the chromosome terminus region and indirectly interacts with FtsZ through two other proteins. We report here that MatP also forms biomolecular condensates in reconstituted systems that mimic the crowded bacterial cytoplasm, on its own or with FtsZ. Our biophysical analyses uncover a direct MatP-FtsZ interaction, which is disrupted by *matS* sites that also regulate MatP condensate formation. These condensates preferentially locate at the surface of lipid droplets, a behavior probably mediated by MatP-lipid binding. GTP triggers assembly of FtsZ polymers from FtsZ-MatP condensates. These polymers are decorated with MatP, but exposure to *matS* sites releases MatP. Such *matS*-responsive MatP biomolecular condensates, regulated by GTP when coassembled with FtsZ, may provide a mechanism for MatP storage

and rapid mobilization that could facilitate MatP's role in spatially regulating cytokinesis. Moreover, sequestration of MatP through phase separation could promote cell entry into dormant states that are able to survive antibiotic treatments.

GRAPHICAL ABSTRACT

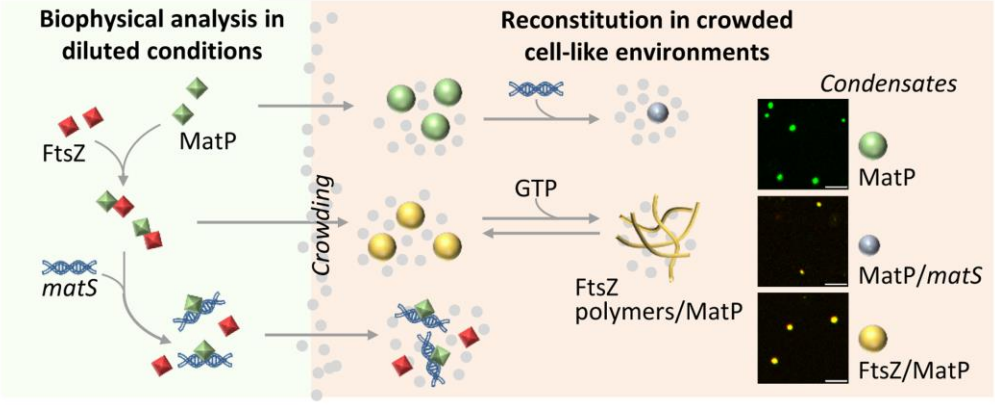

INTRODUCTION

Biomolecular condensation through phase separation is established as a mechanism to regulate cellular function and pathology in eukaryotes (1–3). Although its identification in bacteria is more recent, increasing evidence supports both its key role in providing a mechanism for compartmentalization of these cytoplasms lacking membrane-bound organelles, and additional levels of regulation for multiple cellular processes (4, 5). Biomolecular condensates are dynamic assemblies of a single or various scaffold biomolecules in which others, termed clients, selectively concentrate, providing spatial control to reactions (6, 7). These condensates reversibly form under a narrow range of conditions (8), being favored by multivalency and macromolecular crowding, through volume exclusion or other nonspecific weak interactions (1, 9). In many instances, biomolecular condensation of proteins, often regulated by nucleic acids, enhances cell fitness and survival in response to different kinds of stresses. In the particular case of bacteria, condensates conferring resistance to starvation, heat shock, phage infection, oxidative stress, or treatments with antibiotics have been identified (5, 10), suggesting that these structures may represent attractive new targets for the fight of antimicrobial resistance.

Bacterial cell division proteins from *Escherichia coli*, *Bacillus subtilis* and *Caulobacter crescentus* assemble biomolecular condensates in cytomimetic systems mimicking the crowded bacterial cytoplasm and/or *in vivo*. These condensates are proposed to participate in the orchestration of this essential process ((5) and references therein). Cytokinesis in the model species *E. coli* is achieved through the formation of a Z ring at midcell comprising polymers of the GTPase FtsZ, in coordination with chromosome segregation (11). Spatiotemporal control of the assembly of this ring is ensured by the joint action of mechanisms such as nucleoid occlusion, mediated by the protein SlmA (12), and the Ter linkage exerted by a multiprotein complex comprising the proteins ZapA, ZapB and MatP (13). Besides the GTP-triggered polymers, which laterally interact to form bundles in crowding conditions, FtsZ forms biomolecular condensates strongly promoted by macromolecular crowding (14) and through interaction with the nucleoprotein complexes of SlmA (15). FtsZ condensates and polymers interconvert in response to GTP addition and depletion after GTP hydrolysis, and FtsZ modulators modify the switch between both structures. Thus, SlmA strongly antagonizes FtsZ polymerization favoring condensates (15), whereas ZapA, which does not form condensates on its own but incorporates into the homotypic and heterotypic FtsZ condensates, counteracts the effects of SlmA, tilting the balance towards FtsZ polymers (16). This interplay between biomolecular condensates, polymers and agonists/antagonists of FtsZ has been proposed to contribute to the exquisite regulation of division ring assembly in time and space under normal growth conditions (16). Additionally, since they sequester FtsZ together with a strong polymerization antagonist (SlmA), these division condensates could be among those occurring in dormant cell states tolerant to antibiotics, in which GTP biosynthesis is downregulated and vital processes like division shut down (17, 18). Consistent with this, regrowth delay bodies enriched in FtsZ have been identified in persister cells surviving antibiotic treatment that dissociate when the cells resume growth (19).

The Ter linkage protein MatP, involved in division ring positioning and in the coordination of cytokinesis with chromosome segregation, is a specific DNA binding factor targeting *matS* sites, which are repeated over 20 times at the Ter region of the chromosome (20, 21). *In vivo*, MatP forms a discrete focus that colocalizes with the Ter macrodomain, playing a pivotal role in its organization and compaction. Besides the specific recognition of DNA, the modular

structure of MatP (22) comprises multiple regions of interaction with itself (leading to dimerization), with other proteins and with lipid membranes. Within the Ter linkage, MatP directly interacts through its C-terminal half with ZapB (23), which binds ZapA, a protein known to recognize FtsZ (24). Aside from this canonical sequence of interactions with partner proteins, it has been suggested that ZapB may directly bind FtsZ (25, 26). In *E. coli*, MatP also interacts with the structural maintenance of chromosomes (SMC) complex MukBEF, contributing to normal chromosome organization and timely unlinking of replicated chromosomes, allowing their segregation (27, 28). Thus, MatP delays sister Ter segregation by releasing MukBEF from the Ter region, which limits the availability at this location of Topoisomerase IV that normally removes chromosomal catenanes. MatP has been found to bind lipid membranes, which may play a role in the regulation of its function through modulation of its localization and recognition of other ligands (29).

Here, by reconstitution in crowding conditions and in cell-like systems generated by microfluidics, we show that MatP can form dynamic biomolecular condensates, as revealed by confocal microscopy and turbidity analyses. Condensation is strongly enhanced by FtsZ, with the two proteins forming heterotypic condensates under conditions in which they do not significantly form condensates on their own. An orthogonal approach using fluorescence anisotropy, fluorescence correlation spectroscopy (FCS) and analytical ultracentrifugation (sedimentation velocity, SV) uncovered direct interaction between MatP and FtsZ oligomers and GTP-triggered polymers. We also investigated the impact of *matS* sequences on the assembly of MatP into biomolecular condensates and on the interactions with FtsZ. The formation of dynamic reversible biomolecular condensates by MatP could be instrumental in processes determining bacterial survival of stress conditions, such as quiescent states in which cell division is arrested and the proteins involved are stored in compartments. It could also be relevant for the role of MatP in the positioning of the Z ring and in the organization of the chromosome, regulating its segregation and compaction.

MATERIAL AND METHODS

Reagents

Polar extract phospholipids from *E. coli* were from Avanti Polar Lipids (AL, USA), and stored in chloroform at −20 °C until used. GTP and dextran 500 (500 kDa) were from Merck (NJ, USA). Ficoll 70 (70 kDa) was from GE Healthcare (IL, USA). Alexa Fluor 488 and Alexa Fluor 647 carboxylic acid succinimidyl ester dyes were from Thermo Fisher Scientific Inc. (MA, USA). Analytical-grade chemicals were from Merck.

Protein purification and labeling, and DNA hybridization

FtsZ was purified following the calcium-induced precipitation method (30), and MatP was isolated as described elsewhere (29), to obtain the untagged protein. Proteins were stored in aliquots at -80 °C. For the experiments, MatP was equilibrated in 50 mM Tris-HCl pH 7.5 and 300 mM KCl to avoid protein aggregation, salt content subsequently adjusted to the conditions required for each particular experiment. In the case of FtsZ, the dialysis buffer was 50 mM Tris-HCl pH 7.5, with 5 mM $MgCl_2$ and the specified KCl concentration. FtsZ and MatP were covalently labeled at their amino groups with Alexa Fluor 488 or Alexa Fluor 647 carboxylic acid succinimidyl ester dyes as previously described ((31), FtsZ and (29), MatP). The labeled protein was purified from the excess of dye in the reaction mixture using a HiTrap Desalting column (Cytiva Sweden AB). In all cases, the labeling ratio, calculated from the molar absorption coefficients of the proteins and the dyes, was always below 1 mole of dye per mole of protein.

Single stranded oligonucleotides purified by HPLC containing the *matS19* sequence (AAAGTGACACTGTCACCTT, bases recognized by MatP underlined (20)) or a nonspecific sequence of similar length (AAGTAAGTGAGCGCTCACTTACGT), either unlabeled or labeled with Alexa Fluor 647 or fluorescein in the 5′ end, were obtained from IDT. Hybridization of the complementary oligonucleotides using a thermocycler was described elsewhere (29).

Preparation of samples in crowding bulk solution

The crowding bulk solutions were prepared in Protein LoBind® tubes (Eppendorf) by directly adding the protein(s) to the solution containing the specified crowder, dextran 500 or Ficoll 70. Crowder was previously dialyzed in 50 mM Tris-HCl, pH 7.5 without or with 100 mM or 300 mM KCl and the concentration measured from the refractive index increment as described (32). The final buffer conditions were adjusted to be 50 mM Tris-HCl pH 7.5, 5 mM

$MgCl_2$, 200 g/L dextran and 100 mM KCl (MatP-crowding conditions), for most analysis of MatP condensates and 50 mM Tris-HCl pH 7.5, 1 mM $MgCl_2$, 150 g/L dextran and 200 mM KCl (FtsZ/MatP-crowding conditions), for analysis of FtsZ/MatP condensates, unless otherwise stated. When required, polymerization of FtsZ was triggered by direct addition of GTP.

Turbidity assays and determination of c_{sat}

Turbidity measurements for the study of condensate formation were performed using a Varioskan Flash Plate reader (Thermo Fisher Scientific, MA, USA) following a protocol described elsewhere (14). Samples (85 µL) were measured at 350 nm in 384-well clear polystyrene, flat bottom microplates (Greiner Bio-One) after 30 min incubation at room temperature. Salt shift experiments were conducted measuring the turbidity just after addition of a small volume of a KCl stock solution (2.7 M KCl, in 50 mM Tris-HCl pH 7.5) into the condensates solutions. Samples named "vehicle" refer to those where an equivalent volume of buffer with no KCl (50 mM Tris-HCl pH 7.5) was added instead, accounting for a possible effect derived from the dilution of the protein(s). The concentration threshold for condensate formation, c_{sat}, was determined from the dependence of the turbidity value with protein concentration by fitting a linear model to the data scaling with the protein concentration (0.5-6 µM), as described earlier (14, 33). The c_{sat} value corresponds to the x intercept. Results are the average of at least three independent experiments ± sd. In samples monitored with time to determine the effect of a particular element (*matS*, nonspecific DNA, vehicle or GTP), absorbance data collection started immediately after its addition. Experiments were generally conducted in MatP- or FtsZ/MatP-crowding conditions (see above).

Microfluidics encapsulation

Microfluidic devices were produced by conventional soft lithography (34). Encapsulation procedure involved mixing two aqueous streams in a 1:1 ratio just before reaching the droplet formation junction. For encapsulation of multiple elements, various compositions of the aqueous phases were assayed to account for possible differences derived from incubation times. Thus, the effect of *matS* on MatP was checked both including MatP and

matS in one aqueous phase each or jointly in both. Likewise, characterization of FtsZ/MatP condensates was conducted by including the two proteins together in both aqueous phases or each one in a different solution with analogous results (and, in the latter case and when present, *matS* was included either in the stream with FtsZ or with MatP, with similar results). Polymerization of FtsZ was induced just before encapsulation, adding GTP in the FtsZ-free aqueous solution. Final concentrations within the microdroplets, reached after the mixing of the solutions, were 5 µM MatP and 1 or 2.5 µM *matS* for MatP condensates; 5 µM FtsZ, 3 µM MatP and 1 µM *matS* for FtsZ/MatP condensates; 1 µM labeled elements used as tracers, and 2 mM GTP. Samples were in MatP-crowding conditions for MatP with or without *matS*, or FtsZ/MatP-crowding conditions (see above) when FtsZ was present. The third stream delivered the mineral oil with the *E. coli* lipid mixture (20 g/L), prepared as described earlier (29). Solutions were delivered at constant flows of 150 µL/h (oil phase) and 10 µL/h (aqueous phases) by automated syringe pumps (Cetoni GmbH, Germany), and production in the microfluidic device was monitored with an Axiovert 135 fluorescence microscope (Zeiss). Microdroplets were collected and observed 30 min after production.

Confocal microscopy

Samples, either crowding bulk solutions or microfluidics droplets, were visualized in silicone chambers (Thermo Fisher Scientific) glued to coverslips using a Leica TCS SP5 inverted confocal microscope with a HCX PL APO 63× oil immersion objective (N.A. = 1.4; Leica, Mannheim, Germany). Excitation of Alexa Fluor 488 and Alexa Fluor 647 was with 488 nm and 633 nm laser lines, respectively. Each individual sample was analyzed by registering several images at different observation fields. Samples with condensates were incubated for 30 min before visualization and, when monitoring the effect of additional elements (proteins or DNA) directly added over the sample, they were imaged before and immediately after the addition or at the specified time. Evolution of polymers with time was monitored by preparing several samples with the same composition and adding, after the 30 min incubation, GTP at different times. Samples contained 1 µM proteins and/or DNA labeled with different dyes, unless otherwise stated.

Production of images and data analysis was done with ImageJ (35). Brightness was uniformly increased to the whole image, only in the specified cases, using Microsoft PowerPoint. To

obtain the intensity profiles, always corresponding to the raw images, we applied the straight-line tool of ImageJ through the lines portrayed in the images. For maximum intensity projections and for 3D reconstructions, the Z-projection and 3D-projection tools were applied, again on raw images. The distribution of diameters of the condensates was measured with the particle analysis option of the software, after noise reduction with a Kuwahara filter and threshold correction by visual inspection, as described (14).

Fluorescence correlation spectroscopy (FCS)

FCS measurements were conducted on a Microtime 200 (PicoQuant) time-resolved confocal fluorescence microscope equipped with a pulsed laser diode head (LDH-P-C-485) for excitation, focused into an UPLSAPO 60x Ultra Planapochromat water immersion objective (NA 1.2), as previously described (16). Experiments were done in dilute solution buffer: 50 mM Tris-HCl pH 7.5, 5 mM $MgCl_2$ and 100 or 300 mM KCl, as specified. For FCS measurements, this buffer contained 0.05 g/L BSA (Merck; dialyzed in 50 mM Tris-HCl pH 7.5, 300 mM KCl), to avoid nonspecific adsorption of the proteins to the surfaces during sample preparation, also prevented by using coverslips treated with Vectabond reagent (Vector Laboratories) and polyethylene glycol succinimidyl ester. When present, concentrations were 10 µM MatP (10 nM MatP labelled with Alexa Fluor 488, MatP-Alexa 488, as tracer), 20 µM FtsZ, 5 µM *matS*, unless otherwise stated. Experiments involving FtsZ polymers also contained 2 mM GTP and an enzymatic GTP regeneration system (RS; 2 units/mL acetate kinase and 15 mM acetyl phosphate, both from Merck), to stabilize FtsZ polymers during the measurements (36). Measurements were performed, at least, in triplicates. For each sample, 5 autocorrelation curves were acquired (1 minute each) and globally analyzed using models including a term for the triplet state dynamics with the FFS Data Processor Software (version 2.4 extended, Scientific Software Technologies Center, Belarus (37)). A one-diffusing species model was fitted to the profiles obtained for samples containing only MatP or FtsZ/MatP/*matS*. Quantitative analysis was omitted for samples containing FtsZ/MatP in view of the multiplicity of species present, including very large complexes, as evidenced by analytical ultracentrifugation. Reported diffusion coefficients are the average of three independent measurements ± s.d.

Sedimentation velocity assays (SV)

MatP and FtsZ samples (320 µL), either alone or mixed, with or without *matS* and in dilute solution buffer with 100 mM KCl were centrifuged at 48,000 rpm in an Optima XL-I analytical ultracentrifuge (Beckman-Coulter Inc.) equipped with both UV-VIS absorbance and Raleigh interference detection systems as earlier described (16). Profiles were recorded by absorbance signal at 250 or 280 nm, or at 280 and 493 nm with samples including *matS*-Fl. When specified, 2 mM GTP and the above described GTP regeneration system were included, and profiles were recorded by Raleigh interference. Differential sedimentation coefficient distributions were calculated by least-squares boundary modeling of SV data using the continuous distribution c(*s*) Lamm equation model as implemented by SEDFIT (38). Heterocomplex formation was qualitatively characterized by multi-signal sedimentation velocity (MSSV) with the "multiwavelength discrete/continuous distribution analysis" model in SEDPHAT software (39), that determines the spectral and diffusion-deconvoluted sedimentation coefficient distributions, $c_k(s)$, of the species (40).

Fluorescence anisotropy

Anisotropy experiments were performed in a Spark® Multimode microplate reader (Tecan) with 485 and 535 nm excitation and emission filters, respectively. Samples were prepared in Protein LoBind tubes and transferred to 384-wells black polystyrene (non-binding surface), flat bottom microplates (Corning). The temperature was regulated at 26 °C. FtsZ/MatP binding isotherms were obtained using 50 nM MatP-Alexa 488 as a tracer, in the same buffer used for the FCS experiments, with 100 mM KCl (see above). Reported anisotropy values are the average of three independent replicates ± s.d. Binding analysis was conducted using BIOEQS software (41, 42), with a simple 1:1 model compatible with the data, to obtain apparent *Kd*s corresponding to the concentration of FtsZ at which half of maximum binding is observed, under our experimental conditions. This analysis takes into account the concentration of MatP. An increase in the total fluorescence intensity occurred as the concentration of FtsZ increased, not due to any background signal from FtsZ (background fluorescence was subtracted in all samples). Quenching of Alexa Fluor 488 fluorescence by amino acids, described in previous reports (43), might occur in MatP-Alexa 488 and be reverted by interaction with FtsZ. However, fluorescence lifetime measurements, using the above described Microtime 200 instrument, showed no significant difference in the average

lifetime (around 2.5-2.6 ns) between free MatP and FtsZ/MatP complexes, ruling out dynamic quenching. Since the quenching of Alexa Fluor 488 by amino acids results from either dynamic or both dynamic and static quenching (43), the lack of dynamic quenching proves this option very unlikely. The increase in intensity could be explained, instead, by a reduction of the high tendency of MatP-Alexa 488 to adsorb to surfaces upon increasing FtsZ concentration, which would not affect the average anisotropy at each FtsZ concentration, nor the apparent binding constants, well above the MatP-Alexa 488 concentration. Nevertheless, BIOEQS analyses were also conducted considering FtsZ/MatP complexes with larger intensity than free MatP, rendering binding parameters only slightly different than those in which equal intensity contribution was assumed (apparent ΔG 6.5 ± 0.2 *vs* 7.0 ± 0.2 kcal/mol; apparent K_d 18 ± 6 *vs* 8 ± 3 μM). Uncertainties in the parameters retrieved were calculated with the same software by rigorous confidence limit testing at the 67% level, and error propagation in the case of the apparent K_d.

The effect of *matS* on the FtsZ/MatP interaction was studied using 5 μM FtsZ (with 50 nM FtsZ labeled with Alexa Fluor 488, FtsZ-Alexa 488, as tracer), unlabeled 2.5 μM MatP and 0.65 or 1.25 μM *matS,* in dilute solution buffer with 100 mM KCl. Titrations of FtsZ (5 μM total, 10 nM FtsZ-Alexa 488) with MatP were conducted in dilute solution buffer with 100 or 300 mM KCl. Anisotropy of FtsZ polymers (with 50 nM FtsZ-Alexa 488 as a tracer) in the presence and absence of MatP and/or *matS* was monitored with time, after 0.25 mM GTP addition in FtsZ/MatP-crowding conditions or measured at time 0 (2 mM GTP) in dilute solution buffer with 100 mM KCl. Reported anisotropy values are the average of three independent replicates ± s.d. and depolymerization profiles are representative of, at least, three independent measurements.

RESULTS

MatP forms biomolecular condensates in crowded cytomimetic systems

Confocal images of purified MatP, containing MatP-Alexa 488 as a tracer, in bulk solution with dextran as crowding agent revealed the presence of relatively small round structures compatible with biomolecular condensates (Figure 1a and Supplementary Figure S1a). They

were also observed in the presence of other crowders such as Ficoll (Supplementary Figure S1b), in this case with lower abundance, but not in their absence (Supplementary Figure S1c). This was consistent with the significant turbidity of MatP solutions in the presence of crowders, and the negligible values in dilute solution (Figure 1b). To get some insight into the nature of these MatP structures, we analyzed their response to changes in ionic strength. We found that increased salt content disfavored condensation, reflected in gradually lower turbidity values and reduction in the abundance of the condensates in the images (Figure 1c and Supplementary Figure S2a). This pointed towards a role of electrostatic interactions in the assembly of MatP condensates.

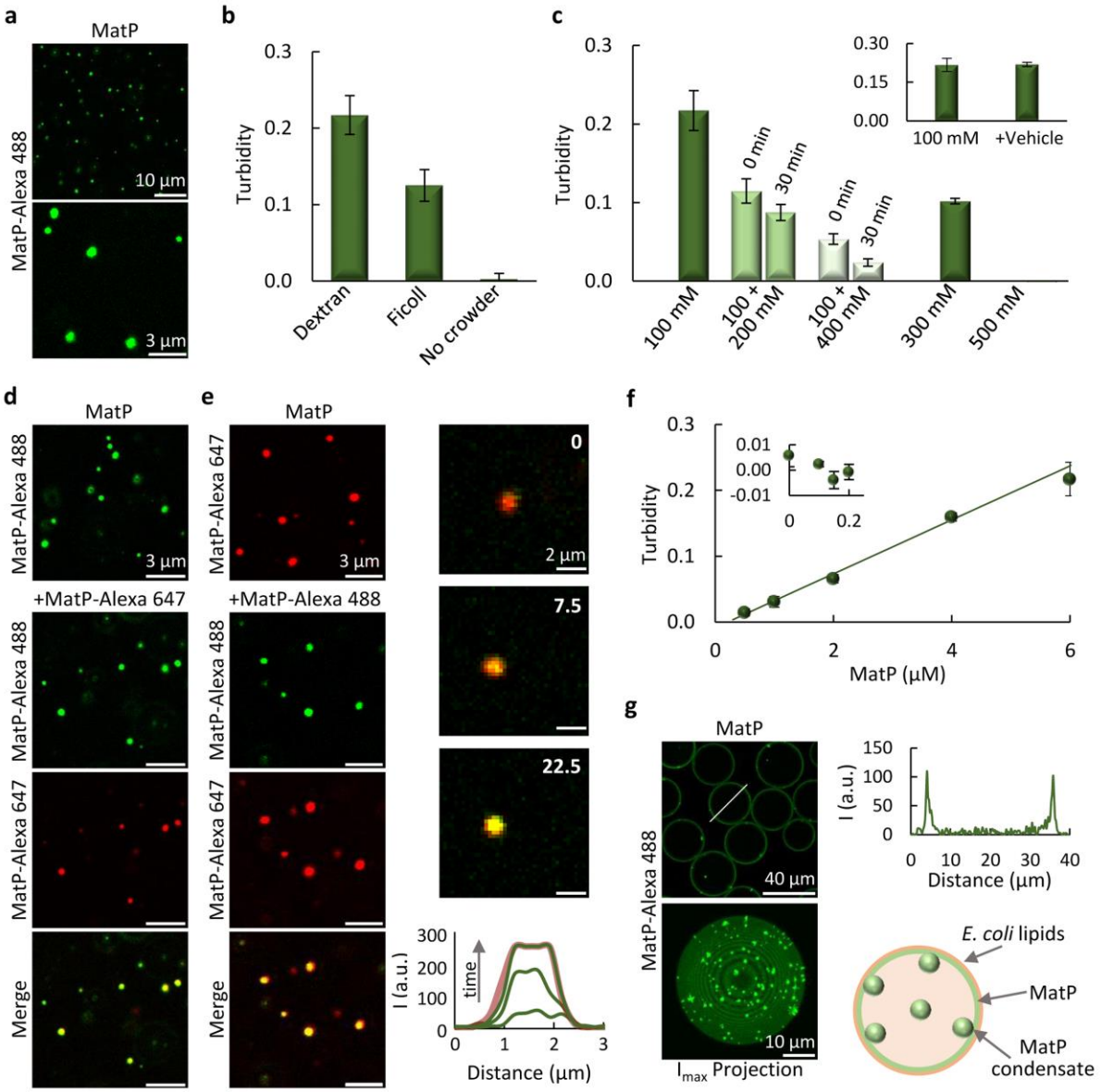

Figure 1. MatP forms biomolecular condensates in crowding conditions. (**a**) Representative confocal microscopy images of MatP condensates. (**b**) Turbidity measurements of MatP samples in dextran (n > 5), Ficoll (n = 3) or in diluted solution (n = 4). (**c**) MatP samples turbidity decrease with the sequential addition of KCl, from 100 mM (n > 5) to 300 and 500 mM monitored at the specified times (n = 3), showing reversibility of MatP condensates. Samples directly prepared at these KCl concentrations are also shown (n = 3). Inset, possible dilution effects were discarded by addition of buffer (no KCl) in a volume equivalent to the highest KCl volume added (vehicle; n = 3). (**d**) and (**e**) Representative images showing incorporation of externally added labeled MatP (0.5 μM) into MatP condensates labeled with a spectrally different dye (0.5 μM), indicating that the condensates are dynamic. Right column in (e) shows the stepwise diffusion of added MatP-Alexa 488 into the condensates at the specified times in seconds (time 0, beginning of the visualization of this particular condensate) with the corresponding intensity profiles below. The profile in the red channel at 22.5 s is shown as reference. (**f**) Turbidity increase with MatP concentration (n = 3 except for 6 μM, n > 5). Line corresponds to a linear model fit, rendering the c_{sat} in the main text. Inset, data below c_{sat} (n ≥ 3). Error bars are within the data symbols in most cases. (**g**) Left, representative images of equatorial section (top) and maximum intensity projection (bottom) of microdroplets containing MatP condensates, located mostly at the lipid membrane. Right, intensity profile corresponding to the line drawn on the image and, below, illustration depicting condensates distribution within the microdroplet. MatP concentration was 5 μM (a, d, e, g) or 6 μM (b, c). Labeled MatP was 1 μM, except when specified. Errors correspond to s.d. All experiments were performed under the MatP-crowding conditions, substituting Ficoll for dextran in (b) as stated.

We also asked whether these structures were dynamic and reversible, features inherent to biomolecular condensates. Condensation was indeed reversible, as addition of supplementary KCl to 100 mM solutions containing the assemblies reduced their amount in the images (Supplementary Figure S2b) and decreased the turbidity values, which approximately matched the turbidity of samples directly prepared at the final salt concentration reached (Figure 1c). Interestingly, turbidity measurements showed a modest

time-dependence of condensate dissociation upon salt addition, explaining the slightly higher abundance of condensates in the images acquired at short times after KCl addition compared with those of condensates directly assembled at the final KCl values (*cf*. Supplementary Figures S2a and S2b). Incorporation of externally added MatP, labeled with Alexa Fluor 647 (MatP-Alexa 647), into condensates containing MatP-Alexa 488 confirmed they were dynamic (Figure 1d and Supplementary Figure S2c). Likewise, MatP-Alexa 488 also incorporated into condensates formed with MatP-Alexa 647 as tracer (Figure 1e and Supplementary Figure S2c). Furthermore, turbidity measurements showed that MatP condensation followed the characteristic behavior associated with protein phase separation in which condensates emerge above a saturation concentration (c_{sat}), with the protein remaining as a single phase below this concentration (2, 9). Thus, negligible turbidity values were obtained at low protein concentration, consistent with the absence of condensates (inset in Figure 1f). At higher MatP concentrations, a linear increase in the turbidity was observed, from which a c_{sat} of 0.2 ± 0.1 μM was retrieved (Figure 1f). Collectively, these experiments indicate that MatP forms dynamic reversible biomolecular condensates driven by crowding.

We further studied the properties of MatP condensates by reconstitution in microfluidics droplets containing dextran as crowder and stabilized in the external oil phase by a monolayer of the lipid ternary mixture found in the *E. coli* inner membrane. We observed that MatP accumulated at this boundary (Figure 1g and Supplementary Figure S3), consistent with the known tendency of the protein to interact with membranes (29). Maximum intensity projections clearly showed defined condensates that, according to the distribution in the equatorial image, were located mainly within the lipid surface of the droplets (Figure 1g and Supplementary Figure S3). These experiments showed that MatP forms condensates in confined cell-like systems displaying crowding and a lipid membrane, with a clear preference for the lipid boundary.

matS **DNA accumulates in MatP condensates, generally disfavoring their formation**

Since nucleic acids are among the strongest modulators of protein phase separation (1), we tested whether the *matS* DNA sequences specifically recognized by MatP influence MatP condensation. Interestingly, the presence of double-stranded (ds) oligonucleotides containing a single *matS* site disrupted the condensates, lowering the turbidity to a higher or lower extent depending on the protein:DNA ratio and on whether *matS* was added to the preformed MatP condensates or incubated with the protein during sample preparation (Figure 2a). Thus, incubation at 5:1 MatP:*matS* molar ratio rendered a turbidity value slightly lower than that of MatP alone, while incubation of MatP with *matS* at a 2:1 ratio resulted in solutions with substantially lower turbidity, indicating that the presence of *matS* prevented significant MatP condensation (Figure 2a and Supplementary Figure S4a). Notably, addition of *matS* into the preassembled MatP condensates had a lower impact, reflected in a modest decrease in the turbidity at a 5:1 MatP:*matS* ratio, and a larger decrease at a 2:1 ratio (Figure 2a and Supplementary Figure S4b). Consistent with the turbidity results, confocal analysis showed lower amounts of condensates when MatP was incubated with *matS* at a 5:1 molar ratio, with samples virtually devoid of condensates at a 2:1 ratio (Figure 2b and Supplementary Figure S4c). An apparent decrease in the amount of condensates was observed when *matS* was added to MatP condensates, at both ratios tested (Figure 2c and Supplementary Figure S4c). Interestingly, colocalization of Alexa Fluor 647 labeled *matS* (*matS*-Alexa 647) with MatP-Alexa 488 (Figures 2b, c) evidenced the partitioning of *matS* into the remaining condensates and suggested that MatP within these structures was still able to bind *matS*. Therefore, *matS* reduced the level of MatP condensation in a concentration-dependent manner, more efficiently when the MatP/*matS* complexes were formed before MatP phase separation.

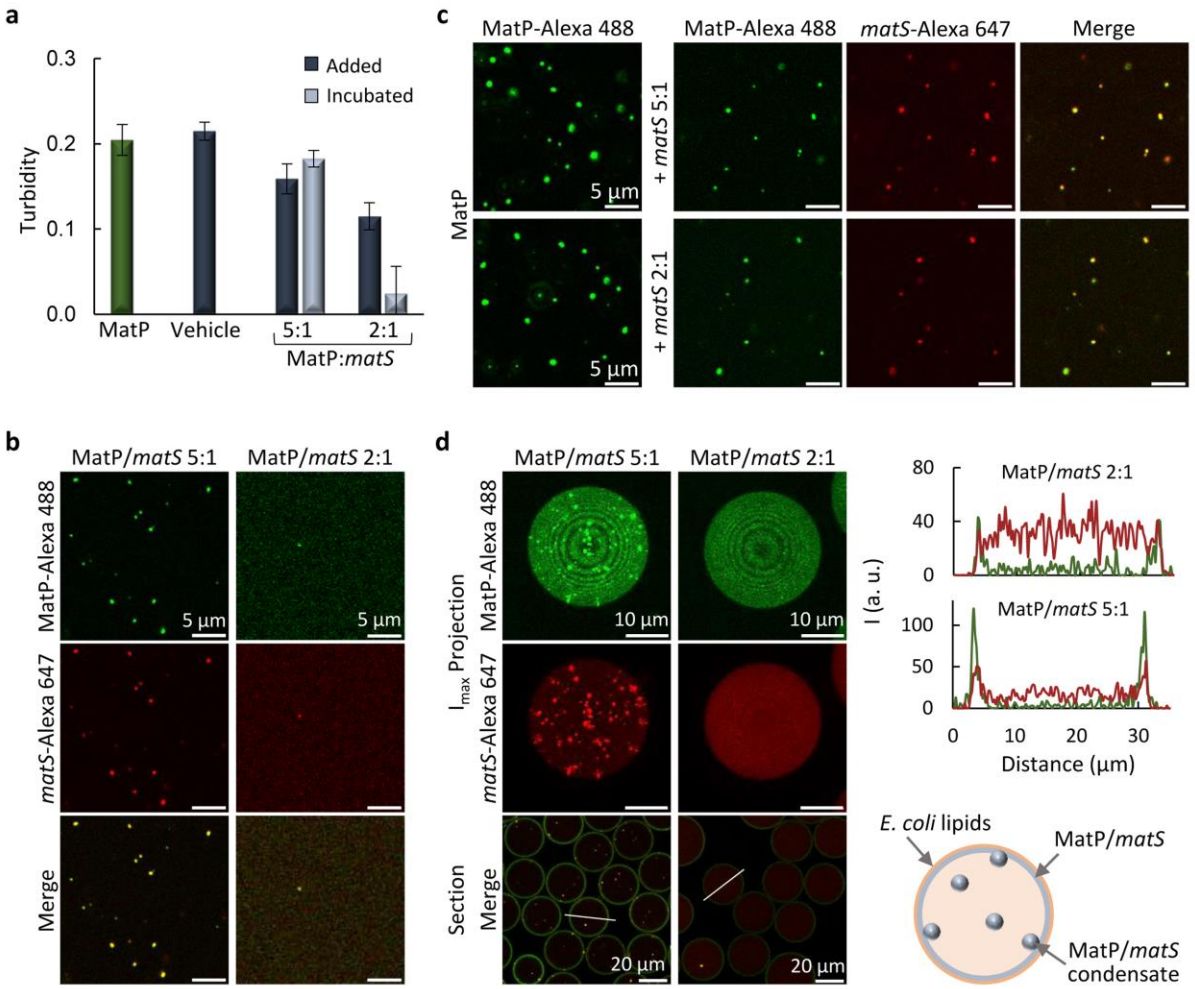

Figure 2. Concentration-dependent modulation of MatP condensates by *matS*. (**a**) MatP turbidity in the absence (n = 5) and presence of *matS,* either added on preformed (30 min-incubated) MatP condensates (measurements taken after 10 min, $n \geq 6$), or incubated with the protein and the crowder for 30 min (n = 3). Possible dilution effects due to the addition of *matS* were ruled out by addition of a buffer volume larger than the largest volume of *matS* added to the MatP solutions (vehicle; n = 3, 10 min). (**b**) and (**c**) Representative confocal images showing the effect of *matS* on MatP condensates. Concentration-dependent inhibition of MatP condensation when incubated with *matS* before condensates assembly (b). Reduction in the abundance of condensates and colocalization of MatP and *matS* in the remaining ones, after addition of *matS* to preformed MatP condensates (c). (**d**) Maximum intensity projections of the independent channels and merge equatorial sections of microdroplets containing MatP incubated with *matS* at the specified ratio. Condensates, found at 5:1 molar ratio, are located both at the lipid membrane and the lumen. Intensity

profiles corresponding to the line drawn on the images are shown on the right, along with a scheme of condensate distribution at 5:1 molar ratio. MatP concentrations were 6 (a) or 5 μM (b, c and d) and *matS* ones corresponded to the specified MatP:*matS* molar ratios. Labeled components were 1 μM. All experiments were performed under the MatP-crowding conditions.

MatP was also co-encapsulated with *matS* inside the above described microfluidics droplets, surrounded by a lipid boundary and with crowder in the lumen (Figure 2d and Supplementary Figure S4d, e). In these experiments, two aqueous streams containing premixed MatP and *matS* were encapsulated. At a 5:1 MatP:*matS* molar ratio, the presence of *matS* did not have a significant impact on the amount of condensates with respect to that observed in its absence (Supplementary Figure S5a), whereas at 2:1 ratio no condensates were detected (Figure 2d). The specific DNA colocalized with the MatP condensates that, still showing a preference for the membrane, increased their abundance in the lumen (Supplementary Figure S5b). Intensity profiles showed accumulation of MatP at the membrane at both MatP:*matS* ratios (Figure 2d and Supplementary Figure S4d), while *matS* was distributed between the lumen and the membrane. These experiments showed that, when at sufficiently high concentration, *matS* hindered MatP phase separation in cell-like systems. At lower concentrations, *matS* DNA fragments partitioned into the condensates, reducing their tendency to assemble at the membrane of the microdroplets.

To evaluate the specificity of the effects found for the *matS* sequences, we tested the impact of ds-oligonucleotides of similar length but lacking this specific site on the MatP condensates (Supplementary Figure S6). A modest reduction in the turbidity was found when the DNA, at 1:1 molar ratio, was incubated with MatP prior to condensate formation, whereas the signal was basically unperturbed upon addition on preassembled condensates even after 30 min (Supplementary Figures S6a and S4b). Accordingly, confocal images showed no variation in the abundance or size of the structures by either addition or incubation with the nonspecific DNA under most conditions assayed (Supplementary Figure S6b, c), with irregular structures only appearing when MatP and the DNA were incubated at a 1:1 molar ratio (Supplementary Figure S6c). Notably, sequences devoid of *matS* sites still partitioned

into the condensates, probably due to nonspecific interactions with MatP favored by the high protein concentration in these structures. These results show that, unlike the specific *matS* sequences, nonspecific DNA did not significantly disrupt MatP condensates, even when it accumulated inside them.

MatP forms heterotypic condensates with FtsZ

FtsZ has been shown to assemble heterotypic condensates in the absence of GTP, through interaction with other bacterial division proteins, acting as scaffolds (15) for additional client proteins (16). Therefore, even though FtsZ is thought to interact with MatP only indirectly (24), we asked whether there could be an interplay between FtsZ and the MatP condensates. Interestingly, addition of FtsZ notably increased the turbidity of MatP solutions (Supplementary Figure S7a), and confocal imaging showed numerous structures (left image in Supplementary Figure S7b), most of which exhibited colocalization of MatP-Alexa 488 and FtsZ labeled with Alexa Fluor 647 (FtsZ-Alexa 647). Under the conditions used to study MatP condensation (MatP-crowding conditions: 200 g/L dextran, 100 mM KCl, 5 mM $MgCl_2$), FtsZ/MatP structures appeared more irregular than the typical round biomolecular condensates (Supplementary Figure S7b). Since these condensates usually form under a narrow range of conditions, and deviation from them often results in either absence of condensation or formation of other types of structures, we decided to explore FtsZ/MatP mixtures at different KCl, $MgCl_2$ and crowder concentrations. Reducing dextran from 200 to 150 g/L (Supplementary Figure S7b) and, even more, increasing KCl to 200 mM, rendered relatively abundant structures, mostly round in shape, at both 1 and 5 mM $MgCl_2$ (Supplementary Figure S8a). Condensates were very sensitive to KCl concentration, while $MgCl_2$ had a lower impact in the range assayed (Supplementary Figure S8a, b).

After this screening, we chose to characterize FtsZ/MatP condensates at 150 g/L dextran, 200 mM KCl and 1 mM $MgCl_2$ (FtsZ/MatP-crowding conditions), where they had the typical appearance associated with biomolecular condensates (Figure 3a). Under these conditions, no condensates were observed in the images of FtsZ alone, in good agreement with previous reports (14), while MatP condensation was negligible (Supplementary Figure S9). This was

further confirmed by turbidity measurements, showing high values indicative of condensate formation only when the two proteins were simultaneously present (Figure 3b). Increasing the KCl content to 300 mM decreased the turbidity to negligible values (Figure 3c), and drastically reduced the number of condensates in the images (Supplementary Figure S10a). As expected, FtsZ/MatP condensates were also formed in the presence of Ficoll (Supplementary Figure S11a), while they did not assemble without a crowding agent (Supplementary Figure S11b). These experiments showed that MatP and FtsZ form condensates when in each other's presence, promoted by crowding and electrostatic forces.

As for the MatP biomolecular condensates, we tested whether the FtsZ/MatP structures were dynamic and reversible. Addition of KCl to already assembled condensates reduced their abundance in the images and the turbidity values (Figure 3c and Supplementary Figure S10b), indicating that they were reversible. Turbidity values reached after salt shifts were similar to those of condensates directly formed at the final KCl value (Figure 3c). FtsZ/MatP condensates assembled with MatP-Alexa 488 as tracer readily incorporated externally added FtsZ-Alexa 647, proving they were dynamic (Figure 3d). This was further confirmed by adding MatP-Alexa 488 on preassembled FtsZ/MatP condensates labeled with FtsZ-Alexa 647 (Supplementary Figure S10c). We also conducted turbidity measurements at a fixed 2:1 FtsZ:MatP ratio, while increasing the overall concentration (Figure 3e). We found that turbidity was negligible at low concentrations, followed by the typical concentration-dependent increase compatible with phase separation at higher concentrations. MatP solutions without FtsZ also exhibited negligible turbidity (Figure 3e) in the concentration interval tested. Altogether, these experiments indicated that MatP and FtsZ formed heterotypic biomolecular condensates in which both proteins behave as scaffold elements, as they both are required for condensation under conditions precluding their individual phase separation, observed under other conditions (see above and (14)).

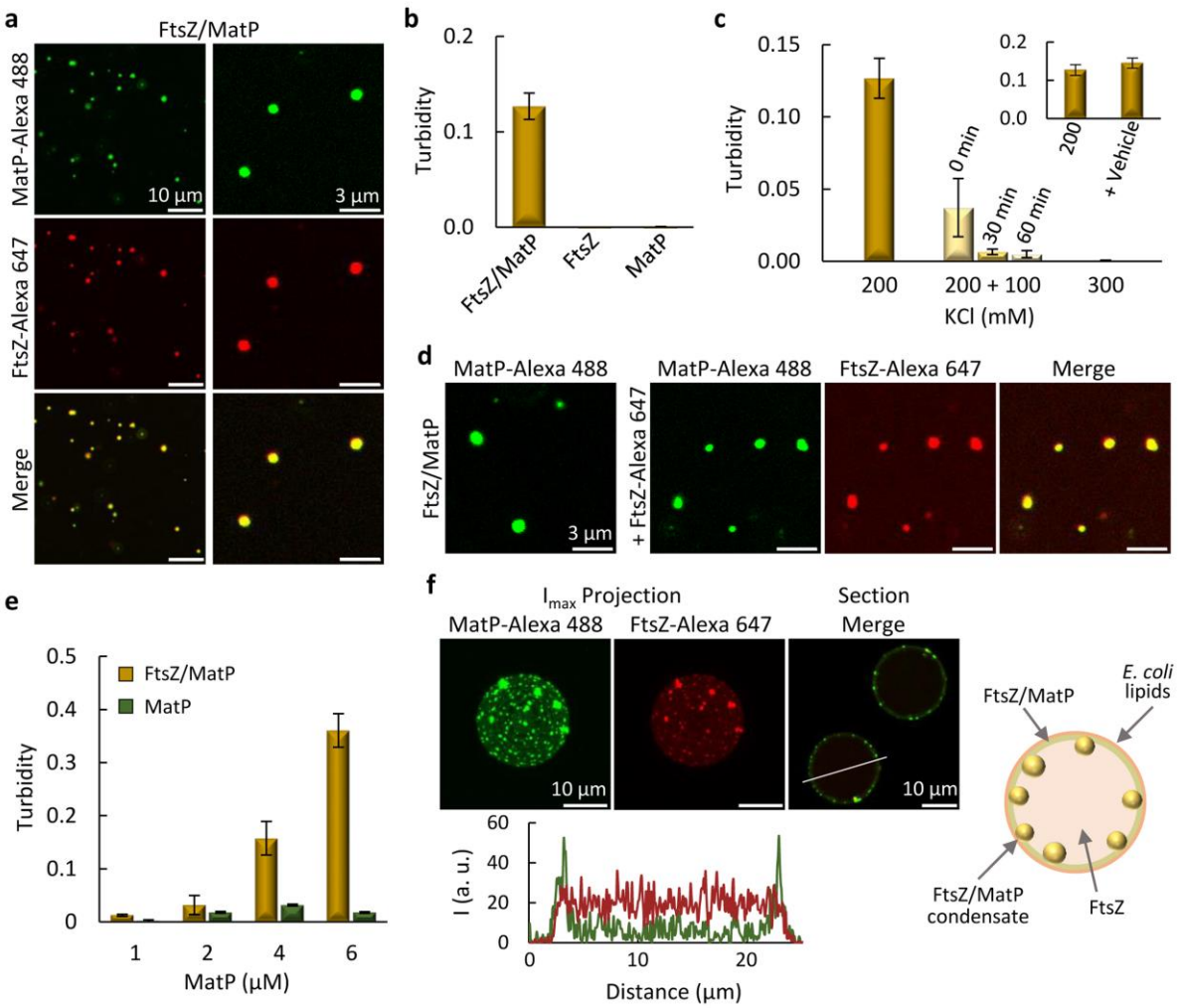

Figure 3. MatP forms heterotypic condensates with FtsZ. (**a**) Representative confocal images showing condensates formed by FtsZ and MatP. (**b**) Turbidity of FtsZ/MatP condensates and lack of signal in samples with FtsZ or MatP, indicative of no condensation. (**c**) Time-dependent decrease in the turbidity of FtsZ/MatP condensates prepared at 200 mM KCl upon addition of KCl up to 300 mM, indicating reversibility of the condensates. Turbidity of samples directly prepared at 300 mM KCl is also shown. Inset shows the absence of a possible dilution effect, by adding an equivalent volume of buffer with no KCl (vehicle). (**d**) FtsZ/MatP condensates incorporate externally-added FtsZ, stating they are dynamic. (**e**) Increase in the turbidity of FtsZ/MatP condensates with protein concentration, keeping a 2:1 (FtsZ:MatP) molar ratio. Turbidity of MatP in the absence of FtsZ is also shown. (**f**) Representative images of the maximum intensity projections of the independent channels and merge equatorial sections of microdroplets containing condensates formed by FtsZ and MatP, mixed at the droplet formation junction. Condensates located mainly at the lipid

membrane. On the right, schematic illustration of condensates distribution within the microdroplets and, below, intensity profiles of the green and red channels corresponding to the line depicted on the image. Concentrations were 5 μM FtsZ, 3 μM MatP and 1 μM labeled components, unless otherwise stated. Data in (b, c) are the average of 3 independent experiments, except for FtsZ/MatP at 200 mM KCl ($n > 5$); in (e) $n = 4$ and $n = 3$ for FtsZ/MatP and MatP samples, respectively, except when MatP was at 6 μM, $n > 5$. Errors are s.d. All experiments were performed under the FtsZ/MatP-crowding conditions, except for salt variations (c).

FtsZ/MatP heterotypic condensates were also analyzed in the cytomimetic platforms displaying crowding, confinement and a lipid membrane. To this end, MatP and FtsZ, with MatP-Alexa 488 and FtsZ-Alexa 647 as tracers, respectively, were jointly encapsulated inside microdroplets generated by microfluidics with dextran as crowder. Numerous condensates in which both proteins colocalized were observed almost exclusively at the membrane (Figure 3f and Supplementary Figure S12a). As in the absence of MatP, FtsZ outside the condensates could also be found homogeneously distributed in the lumen, and also at the membrane (*cf.* Figure 3f and Supplementary Figure S12b, and intensity profiles therein), whereas MatP was mostly at the membrane, either in the form of condensates or as a continuum, with low intensity detected in the lumen. Analogous results were obtained when encapsulating the preformed FtsZ/MatP condensates or when solutions containing each of the proteins were mixed at the droplet formation junction, to trigger heterotypic condensate assembly just before encapsulation (*cf*. Figure 3f and Supplementary Figure S12c). These experiments showed that FtsZ and MatP form condensates also in confined and crowded cell-like systems, with high preference for the lipid membrane.

Negative regulation of condensation by *matS* is also sustained for the FtsZ/MatP condensates

We next asked whether the *matS* sequences specifically bound by MatP modulated the formation of FtsZ/MatP biomolecular condensates, in the same way or differently than that

observed with the MatP homotypic condensates. We found that, at a 5:3:1 FtsZ:MatP:*matS* molar ratio, FtsZ/MatP condensates were also disrupted by ds-oligonucleotides harboring a *matS* site, which largely reduced the turbidity in the samples, more efficiently when preincubated with the two proteins (Figure 4a and Supplementary Figure S13a). Images also showed a considerable reduction in condensate abundance and size when *matS* was added over the preformed condensates (Figure 4b), and basically no condensates in samples in which *matS* was included in the FtsZ/MatP solutions from the beginning (Figure 4c and Supplementary Figure S13b). No condensates were observed either upon co-encapsulation of *matS* with the two proteins, at the same molar ratio as above, in microdroplets with crowding and a lipid membrane (Figure 4d). FtsZ was distributed between the membrane and the lumen, essentially as when encapsulated on its own, i.e. in the absence of MatP and *matS* (Supplementary Figure S12b), the latter localizing primarily in the lumen of the droplet. Hence, the specific DNA recognized by MatP inhibited the formation of condensates both in bulk crowded solution and in cell-like platforms.

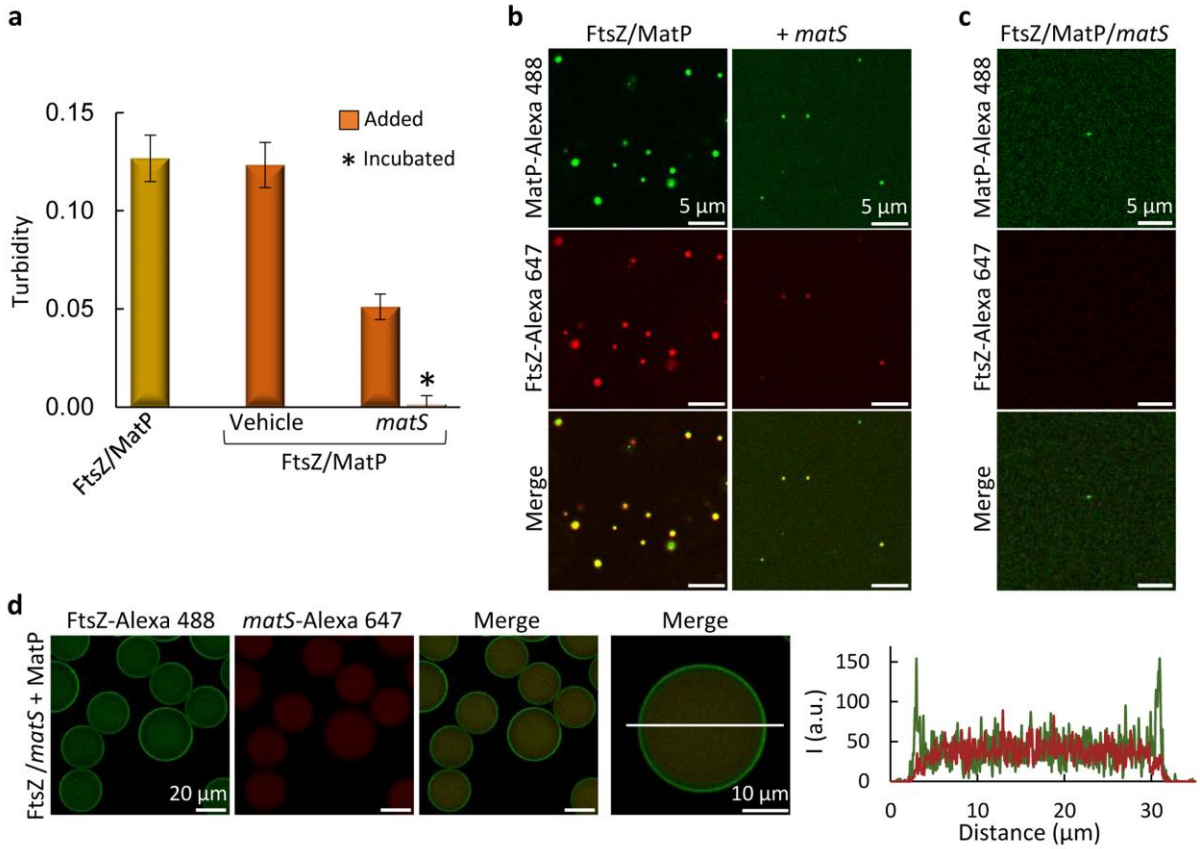

Figure 4. Negative effect of *matS* on FtsZ/MatP condensates. (**a**) Turbidity of FtsZ/MatP condensates decreases by the presence of *matS*, either incubated during sample preparation or by direct addition over the preformed and 30 min-incubated condensates. Sample dilution effects were discarded by addition of the equivalent volume of buffer (vehicle). Samples were measured 10 min after the specified addition. Data are the average of three independent experiments ± s.d. (**b**) and (**c**) Confocal images of FtsZ/MatP condensates before and after *matS* addition (b) and when FtsZ/MatP/*matS* were incubated from the beginning (c). (**d**) Microdroplets containing the two proteins and *matS,* showing lack of condensates. Solution containing FtsZ/*matS* met that containing MatP at the droplet formation junction of the microfluidic device. On the right, intensity profiles corresponding to the green and red channels obtained from the line drawn in the image. Concentrations were 5 μM FtsZ, 3 μM MatP and 1 μM *matS* and labeled components. All experiments were performed under the FtsZ/MatP-crowding conditions.

FtsZ and MatP directly interact and *matS* inhibits the complexes

The formation of heterotypic FtsZ/MatP biomolecular condensates under conditions at which the individual proteins cannot phase separate strongly suggests an interaction between them, which would increase the multivalency rendering the system more prone to condensation. To test this hypothesis, we combined orthogonal biophysical methods (FCS, fluorescence anisotropy and SV), to probe the interaction between FtsZ and MatP in dilute solution.

FCS measurements of MatP, with MatP-Alexa 488 as tracer, showed autocorrelation curves (Figure 5a) described with a single diffusion coefficient *D* (69 ± 2 $\mu m^2/s$) close to that for a MatP dimer (66 $\mu m^2/s$), calculated from the experimentally determined sedimentation coefficient, using Svedberg equation (s = 2.5 S, (29), and see below) and the theoretical mass (~35 kDa). At 100 mM KCl, addition of unlabeled FtsZ shifted the profiles to longer timescales (Figure 5a) because of the formation of large FtsZ/MatP complexes, with some variability in the profiles even for replicates from the same sample. Upon incubation of the two proteins with the specific DNA sequence at 2:1 MatP:*matS* molar ratio, autocorrelation

profiles were superimposable with those of solely MatP (Figure 5a), meaning that the presence of the DNA inhibited the formation of the detected protein heterocomplexes. At 300 mM KCl, profiles of MatP with and without FtsZ overlapped (Figure 5a), indicating that the formation of large (or FCS-detectable) FtsZ/MatP heterocomplexes was disfavored at this higher ionic strength. Therefore, FCS analysis revealed the formation of higher order complexes between MatP and FtsZ involving electrostatic interactions and hindered by *matS*.

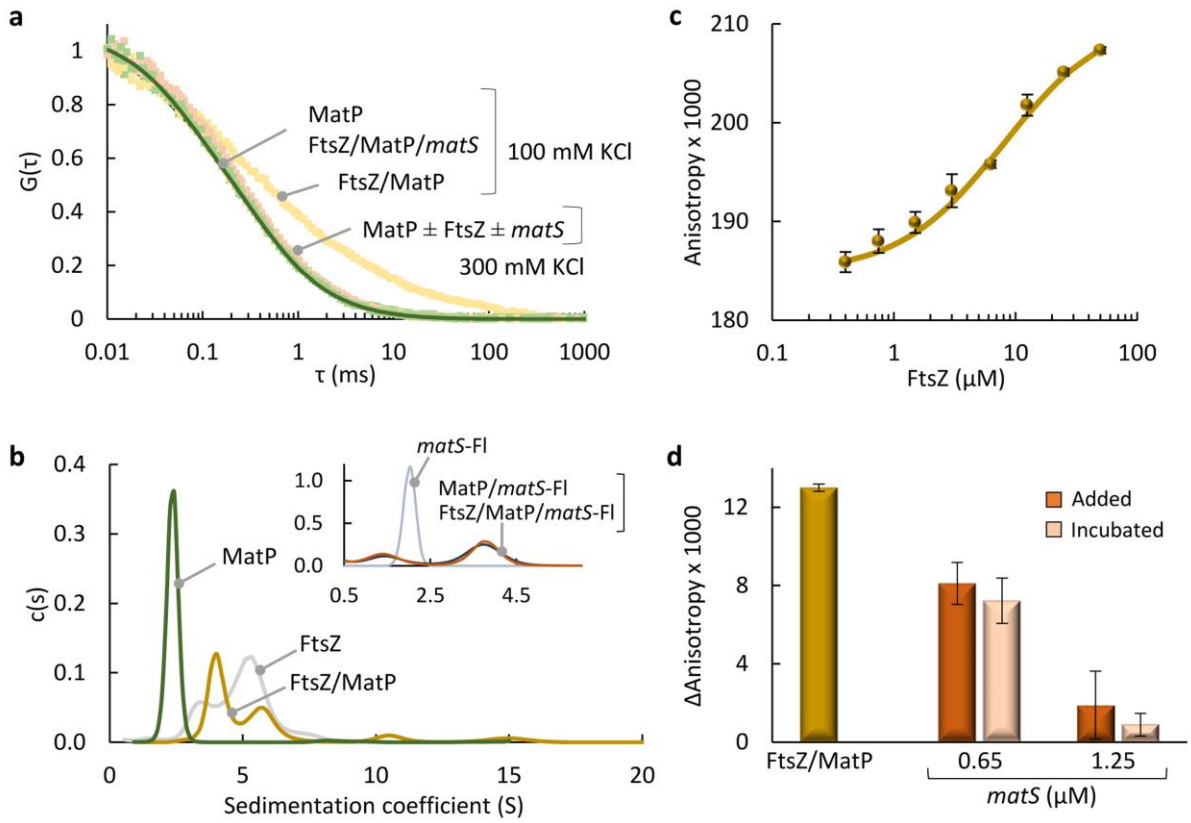

Figure 5. MatP binds to FtsZ through an interaction modulated by *matS*. (**a**) Normalized FCS autocorrelation curves of MatP (10 μM; 10 nM MatP-Alexa 488) and MatP with FtsZ (20 μM) in the presence and absence of *matS* (5 μM) at the specified KCl concentrations (n = 3). Solid line corresponds to the fit of the model described in Materials and Methods. (**b**) Sedimentation velocity analysis of samples containing MatP and FtsZ, alone or combined, followed at 280 nm. Inset, SV profiles of samples containing *matS*-Fl with MatP or with FtsZ/MatP followed at 493 nm. The distribution of *matS*-Fl alone is shown for comparison. Besides other species remaining in solution, FtsZ/MatP samples contained a large fraction of higher order complexes fully sedimenting before the final speed of the assay was reached. The concentrations used were 20 μM FtsZ, 7 μM MatP and 3.5 μM *matS*-Fl. (**c**) Fluorescence

anisotropy binding titrations of MatP (50 nM MatP-Alexa 488, 96 nM total MatP) with FtsZ. Solid line is the best fit of the model specified in the main text, rendering an apparent K_d = 8 ± 3 μM (or 18 ± 6 μM, considering intensity changes, see Materials and Methods for analysis details). (**d**) Change of the fluorescence anisotropy of FtsZ (5 μM, 50 nM FtsZ-Alexa 488) in the presence of MatP (2.5 μM) with and without *matS* (0.65 or 1.25 μM), either incubated for 30 min with the proteins or added over the previously incubated proteins. Data in (c, d) are the average of three independent replicates ± s.d. All the experiments were performed in dilute solution buffer with 100 mM KCl, unless otherwise stated.

The interaction between the two proteins and the effect of *matS* on the complexes were further analyzed by SV. As mentioned above, MatP sedimented as a dimer (2.5 S; Figure 5b and (29)), while FtsZ solutions contained a mixture of species (Figure 5b) consistent with its tendency to form oligomers of variable size (30). Sedimentation coefficient distributions of samples containing both proteins showed the complete disappearance of the peak corresponding to MatP, and the presence of two peaks partially overlapping with those of FtsZ alone, with a substantially lower intensity signal in the higher sedimentation peak (Figure 5b). Multisignal analysis of profiles recorded at two wavelengths revealed that these peaks contained both MatP and FtsZ (Supplementary Figure S14a). Interestingly, we detected a large fraction (∼50%) of higher order complexes that fully sedimented before reaching the final speed of the assay. The effect of specific DNA on the FtsZ/MatP complexes was analyzed by including fluorescein-labeled *matS* (*matS*-Fl) in the samples. Sedimentation coefficient distributions of *matS*-Fl and unlabeled MatP showed a major peak at 3.8 S, corresponding to MatP:*matS* complexes as previously described (29), and a minor amount of free *matS* (inset in Figure 5b). This distribution was not modified in the presence of FtsZ (inset in Figure 5b), indicating that all MatP was still available to form complexes with *matS* and ruling out the formation of FtsZ/MatP complexes, in good agreement with FCS results. Therefore, SV analysis confirmed the interaction between MatP and FtsZ and the inhibition by *matS*.

The affinity of the FtsZ/MatP complexes was evaluated through fluorescence anisotropy binding titrations of MatP (containing MatP-Alexa 488 as a tracer) with increasing

concentration of unlabeled FtsZ. Analysis of the concentration-dependent increase in the anisotropy associated with heterocomplex formation (Figure 5c) rendered an apparent K_d of ~10-20 μM (see Materials and Methods for analysis details), representing the concentration of FtsZ at which half of the maximum binding is observed under these experimental conditions. Fluorescence anisotropy was also used to evaluate the effect of *matS* on the interaction. Addition of MatP to FtsZ (containing FtsZ-Alexa 488 as tracer) resulted in an increase in the measured anisotropy (Figure 5d and Supplementary Figure S14b) indicative of complex formation. Incubation of the two proteins with *matS* or addition of the DNA sequence to the preformed complexes had a similar concentration-dependent inhibition of the FtsZ/MatP interaction, reflected in anisotropy values progressively approaching those of free FtsZ (Figure 5d). Finally, the anisotropy was insensitive to the addition of MatP to labeled FtsZ at 300 mM KCl (Supplementary Figure S14b), a result compatible with a lack of interaction under these conditions. These experiments showed that *matS* was able to inhibit the formation of FtsZ/MatP complexes in solution and to dissociate those already formed.

Taken together, the orthogonal biophysical analyses proved the formation of heterocomplexes of moderate affinity between FtsZ and MatP including large complexes, with electrostatic forces contributing to their formation and *matS* causing their disruption.

FtsZ within FtsZ/MatP biomolecular condensates reversibly forms GTP-triggered filaments decorated with MatP

The ability for GTP-triggered assembly and GTP hydrolysis are hallmarks of FtsZ functionality retained in its previously described homotypic and heterotypic biomolecular condensates, which interconvert with bundles of polymers upon GTP addition and depletion in crowding conditions (14–16). To test whether this was also the case for the FtsZ/MatP condensates, we added GTP to condensates with FtsZ-Alexa 647 and MatP-Alexa 488 as tracers. This resulted in the formation of bundles coexisting, and interconnected, with condensates (Figure 6a, t = 0-20 min). The bundles were initially weakly detected (t = 0) but, after a few minutes (t = 10), they were visible in both the green and red channels, and signal colocalization strongly suggested that MatP incorporated into the FtsZ bundles. At this point, the number of

condensates was significantly reduced while, as time passed, the polymers disbanded because of GDP accumulation due to GTP hydrolysis by FtsZ, and condensates where both proteins colocalized reassembled (Figure 6a, t >30). Curiously enough, reassembled condensates seemed to be larger and less abundant than the ones from which polymerization was triggered (Figure 6a, *cf*. GDP and t = 60-90) to evolve, with time, acquiring a size closer to that of the prepolymerization condensates (Figure 6a, *cf*. GDP and t = 120). Incorporation of MatP to FtsZ bundles was further confirmed through experiments in which MatP was added to preformed FtsZ polymers (Figure 6b), allowing their inspection in the absence of condensates. Under these conditions, MatP signal corresponding to the MatP-Alexa 488 tracer colocalized with that of the FtsZ polymers, containing FtsZ-Alexa 647. The presence of MatP seemed to prolong the lifetime of the FtsZ polymers as, in its absence, no polymers could be detected 10 minutes after GTP addition (Supplementary Figure S15).

The response of the FtsZ/MatP condensates to GTP was also monitored by turbidity (Figure 6c). A decrease in this parameter was found at short times after addition of GTP, consistent with the formation of bundles and the concomitant dissociation of the FtsZ/MatP condensates, as previously described for other FtsZ biomolecular condensates (14, 16). Polymerization arising only from the protein outside the condensates would have increased the turbidity rather than decreased it, because the overall signal would have been then contributed by both the intact condensates and the newly formed polymers. The turbidity values reached a minimum at ~10 min, time at which the images showed mainly polymers with a few condensates (Figure 6a, t = 10). The signal increased afterwards, plateauing at ~30 minutes and approximately maintaining the value reached during the observation time (Figure 6c). This was compatible with the reassembly of condensates upon polymer disassembly, as observed in the images (Figure 6a, t >30 min). In the absence of MatP, addition of GTP to samples containing FtsZ induced the typical rapid increase in turbidity due to the assembly of crowding-induced bundles from the unassembled protein, which did not form condensates under these conditions, followed by a signal drop to the initial values with polymers disassembly (Figure 6c). The low signal precluded accurate determination of how long the polymers lasted.

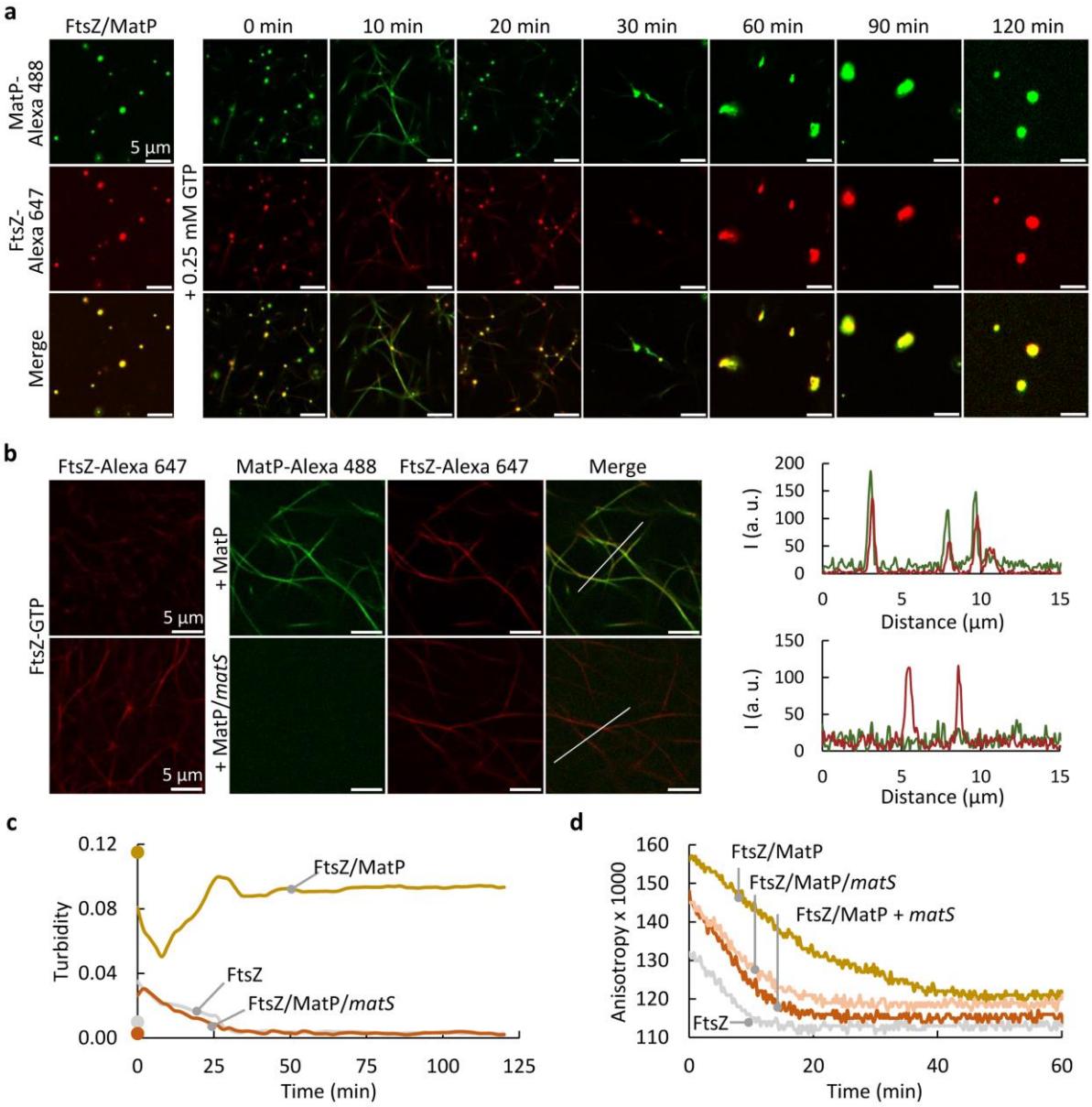

Figure 6. MatP decorates GTP-driven FtsZ bundles, assembled in solution or when evolved from FtsZ/MatP condensates, and dislodges in the presence of *matS*. (**a**) Representative confocal images of FtsZ/MatP condensates before and after GTP addition and time-evolution showing condensate reassembly. (**b**) Confocal images of FtsZ bundles triggered by addition of 2 mM GTP before and after addition of MatP (top) or MatP/*matS* (bottom). On the right, intensity profiles of the red and green channels corresponding to the lines depicted in the images, evidencing colocalization of both proteins in the polymers in the absence of *matS*. (**c**) Representative turbidity profiles of FtsZ-GTP samples as compared to FtsZ-GTP/MatP with or without *matS* (n = 3). Values prior to polymerization are represented as dots at 0 min (n = 3). (**d**) Representative depolymerization profiles of FtsZ (50 nM FtsZ-Alexa 488) in the presence

of MatP or MatP/*matS* (n > 5). The effect of the addition of *matS* (+*matS*) to FtsZ/MatP immediately after polymerization was also tested (*n* = 3). All the experiments were performed in FtsZ/MatP-crowding conditions. When present, the concentrations of FtsZ, MatP and *matS* were 5, 3 and 1 μM, respectively. In (a) and (b) concentration of labeled components was 1 μM. Except in (b), polymerization was induced by addition of 0.25 mM GTP.

Fluorescence anisotropy experiments conducted in parallel, with FtsZ-Alexa 488 as a tracer, showed an increase in the anisotropy value upon GTP addition to FtsZ/MatP condensates compatible with the formation of FtsZ filaments, as previously described (16, 31). With time, the anisotropy decreased due to the polymers dissociation, plateauing after around 30-40 minutes (Figure 6d), in fair agreement with confocal microscopy and turbidity analysis. Notably, the fluorescence anisotropy in the presence of MatP was higher during the whole time interval than in its absence, reflecting the presence of condensates (absent from the FtsZ only samples) and/or the formation of larger or more rigid polymers. In the absence of MatP, the anisotropy reached a plateau at ~ 10 min (Figure 6d), suggesting a shorter duration of the polymers than in the presence of MatP, in accordance with confocal images.

Taken together, the turbidity, confocal and anisotropy experiments showed that the FtsZ/MatP biomolecular condensates evolved towards polymers in the presence of GTP and reassembled upon GTP exhaustion, analogously to other FtsZ-containing biomolecular condensates. Moreover, these results strongly suggested that MatP binds to the FtsZ bundles and that the polymers disassembly was retarded.

We also studied the behavior of the FtsZ polymers when co-encapsulated with MatP inside microdroplets with dextran as crowder and a lipid boundary. Polymerization was triggered by GTP at the droplet formation junction of the microfluidic device just before encapsulation. Confocal images showed the colocalization of FtsZ-Alexa 647 and MatP-Alexa 488 tracers, at the membrane of the microdroplets (Figure 7a). Polymers in which both proteins colocalized were clearly observed in the maximum intensity projections, and equatorial sections and 3D reconstructions evidenced their presence mostly at the membrane surface (Figure 7a and

Supplementary Figure S16a, and Movie 1). In the absence of MatP, FtsZ polymers were also found at the membrane, but their presence in the lumen was more evident than with MatP (Supplementary Figure S16b, and Movie 2), suggesting that the FtsZ/MatP interaction shifted them towards the membrane. Hence, MatP decorated FtsZ polymers also when reconstituted in cell-like microdroplets, increasing their tendency to locate at the lipid membrane.

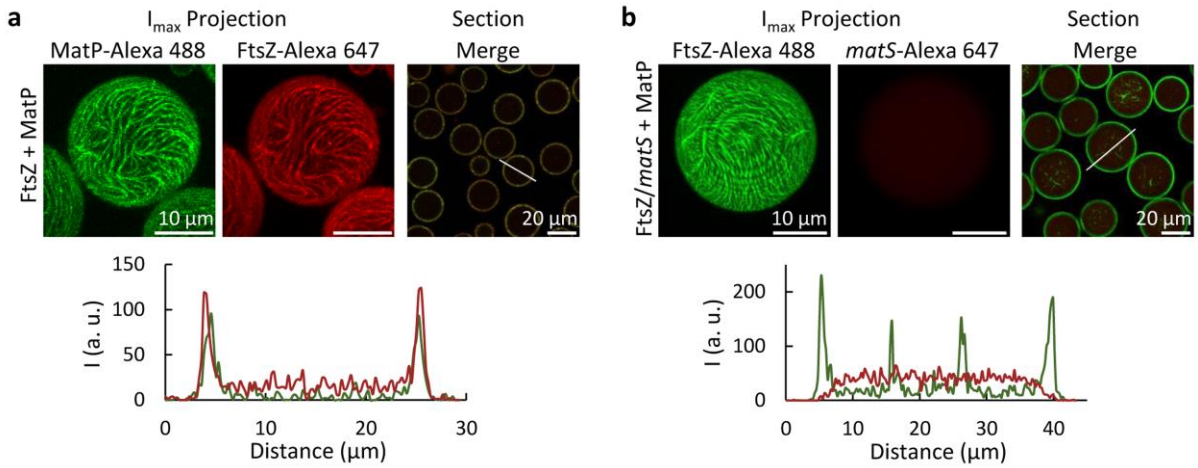

Figure 7. Reconstitution of GTP-triggered FtsZ bundles with MatP and *matS* in microfluidics droplets. (**a, b**) Representative confocal images of the maximum intensity projections of the independent channels and, on the far right, merge equatorial sections of microdroplets containing FtsZ polymers and MatP in the absence (a) and presence of *matS* (b). Intensity profiles of the green and red channels obtained along the line in the corresponding images are also shown. FtsZ and MatP (in the absence of *matS*) or FtsZ/*matS* and MatP met at the droplet formation junction of the microfluidic device. Concentrations were 5 µM FtsZ, 3 µM MatP and 1 µM *matS* and labeled components. Polymerization was triggered with 2 mM GTP just before encapsulation. Experiments were performed under the FtsZ/MatP-crowding conditions.

Specific DNA sequences dissociate MatP from the FtsZ bundles in crowding conditions

The experiments described above showed that MatP incorporated into the GTP-induced FtsZ bundles formed in the presence of crowding agents, modifying their disassembly kinetics and distribution in cytomimetic systems. Hence, we asked if the DNA sequences containing

matS sites recognized by MatP could modify these observations. Incubation of MatP with *matS* prevented incorporation of MatP into the FtsZ polymers, the fluorescence signal in the corresponding channel appearing homogeneously distributed in the images (Figure 6b, bottom). Supporting these findings, the turbidity profiles depicting the evolution of FtsZ/MatP/*matS* upon addition of GTP practically overlapped with those of FtsZ alone (Figure 6c), consistent with the disruption of the FtsZ/MatP condensates (prior to the addition of the nucleotide) and the *matS*-induced inhibition of MatP binding to the polymers. Moreover, the notable difference between the anisotropy depolymerization profiles of FtsZ/MatP and FtsZ in the absence of MatP was largely reduced when the two proteins were incubated with *matS* (Figure 6d). Likewise, addition of *matS* to FtsZ polymers decorated with MatP induced the dissociation of the latter from the polymers (Supplementary Figure S17). No incorporation of MatP or *matS* to the FtsZ polymers was found when polymerization was triggered from samples containing the two proteins and the DNA (Supplementary Figure S18). Therefore, *matS* precluded incorporation of MatP to the FtsZ polymers, being also able to remove the protein when already bound.

When *matS* was included in the FtsZ/MatP mixtures encapsulated in lipid-stabilized microdroplets with crowder in their interior, the GTP-triggered FtsZ polymers were observed at the membrane and also in the lumen (Figure 7b and Supplementary Figures S16c and S19), adopting a distribution similar to that found in the absence of MatP (Supplementary Figure S16b). MatP was detected principally at the membrane (Supplementary Figure S19 and Movie 3), while *matS* remained homogeneously distributed in the lumen (Figure 7b and Supplementary Figure S16c). Neither MatP nor *matS* colocalized with the FtsZ polymers (Figure 7b and Supplementary Figure S19). These experiments showed that the inhibition of MatP accumulation at FtsZ bundles by *matS* occurred also under cytomimetic conditions.

MatP also binds the polymeric form of FtsZ, and specific DNA disrupts the complexes

Experiments performed in crowding conditions suggested the interplay between MatP and FtsZ is also maintained when FtsZ is forming bundles, consistent with an interaction. This prompted us to determine whether MatP could also bind the single-stranded protofilaments

FtsZ forms in dilute solution (44–46). FCS experiments with MatP-Alexa 488 as a tracer showed a displacement of the profiles of dimeric MatP (see above) to longer times in the presence of FtsZ polymers (Figure 8a), induced by GTP and stabilized by an enzymatic regeneration system (RS, (36)), to keep them in solution during sufficient time to be characterized. Sedimentation velocity analysis of samples containing the two proteins with GTP and RS showed the formation of very large complexes that sedimented in a large proportion before reaching the final speed of the assay, in contrast with the FtsZ polymers in the absence of MatP (Figure 8b). Finally, fluorescence anisotropy measurements of FtsZ polymers (with FtsZ-Alexa 488 as tracer) showed a shift by MatP to higher anisotropy values (Figure 8c), a result compatible with the formation of larger or more rigid species. Altogether, these experiments showed MatP binding to the FtsZ polymers, forming complexes larger than the FtsZ polymers in the absence of MatP.

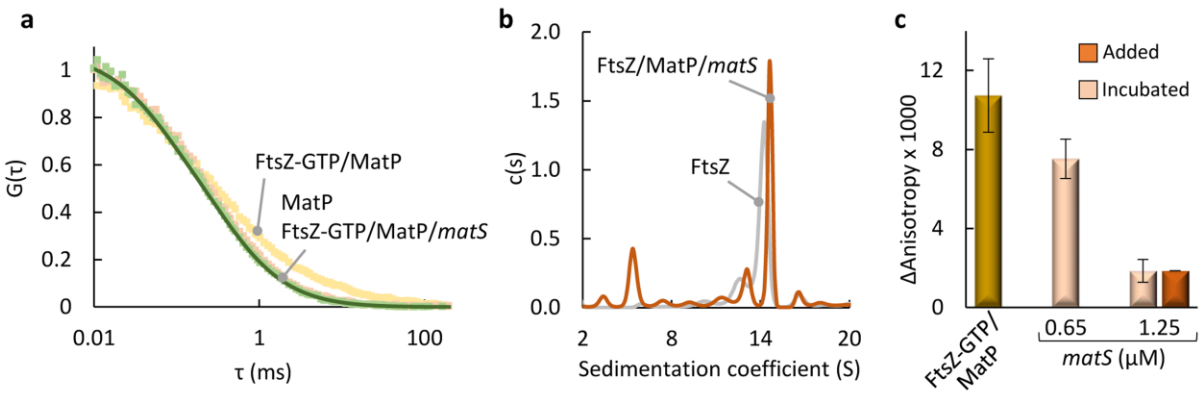

Figure 8. MatP interacts with GTP-triggered FtsZ polymers and *matS* disrupts these complexes. (**a**) Normalized FCS autocorrelation curves of MatP (10 nM MatP-Alexa 488 tracer), in the absence and presence of FtsZ and with or without *matS* (n > 5). Solid line corresponds to the fit of the model indicated in the main text. (**b**) SV interference distribution of FtsZ polymers with or without MatP/*matS*. FtsZ/MatP samples contained very large complexes that substantially sedimented before reaching the final speed of the assay, in addition to other species that remained in solution. Evolution of the sample during the experiment precluded quantitative analysis to obtain sedimentation coefficient distributions. (**c**) Change of the fluorescence anisotropy of FtsZ polymers (50 nM FtsZ-Alexa 488) with MatP in the absence and presence of *matS*. Value after addition of *matS* at the highest concentration right after polymerization of FtsZ/MatP samples is also shown. Experiments

are representative of 3 independent replicates (a, b) or the average of 3 independent experiments ± s.d. (c), and were conducted in dilute solution buffer with 100 mM KCl. Concentrations were 10 µM (a), 5 µM (b) or 2.5 µM (c) MatP; 20 µM (a), 10 µM (b) or 5 µM (c) FtsZ; 5 µM (a), 2.5 µM (b) or as specified (c) *matS*. Polymerization was triggered by addition of 2 mM GTP with (a, b) or without RS (c).

We also probed the effect of the *matS* sequence on the binding of MatP to the FtsZ polymers and found it disrupted the complexes detected in the FCS experiments, leading to profiles approximately matching those of samples containing only MatP, the labeled element in these assays (Figure 8a). Analogously, the sedimentation coefficient distributions of the FtsZ polymers were roughly the same as those observed upon incubation of FtsZ with MatP/*matS* and triggering assembly with GTP (Figure 8b). Moreover, a concentration-dependent antagonistic effect of *matS*, whether added prior to or after triggering polymerization of the FtsZ/MatP mixtures, was also observed by anisotropy. The anisotropy values of MatP/FtsZ/GTP gradually approached that of the FtsZ polymers in the absence of MatP, as the concentration of *matS* in the samples increased (Figure 8c). Therefore, *matS* blocked MatP binding to the FtsZ protofilaments in a concentration-dependent manner.

DISCUSSION

There is increasing evidence that phase separation phenomena leading to biomolecular condensation play a crucial role in the regulation of essential processes in bacteria, including cell cycle events. Here, we show that the bacterial protein MatP, which participates in both Z ring positioning and coordination of cell division and chromosome segregation, undergoes dynamic and reversible biomolecular condensation in crowding cytomimetic conditions (Figure 9a). These novel assemblies are negatively regulated by *matS* DNA sites that partition into them, also when formed at lipid membranes, for which the protein displays affinity. Accumulation of FtsZ into MatP condensates suggests a direct interaction between these two proteins, confirmed by biophysical analysis in dilute solution, that facilitates phase separation

through heterotypic condensation involving both proteins. MatP also interacts with FtsZ polymers elicited by GTP, but *matS* sites efficiently block this interaction.

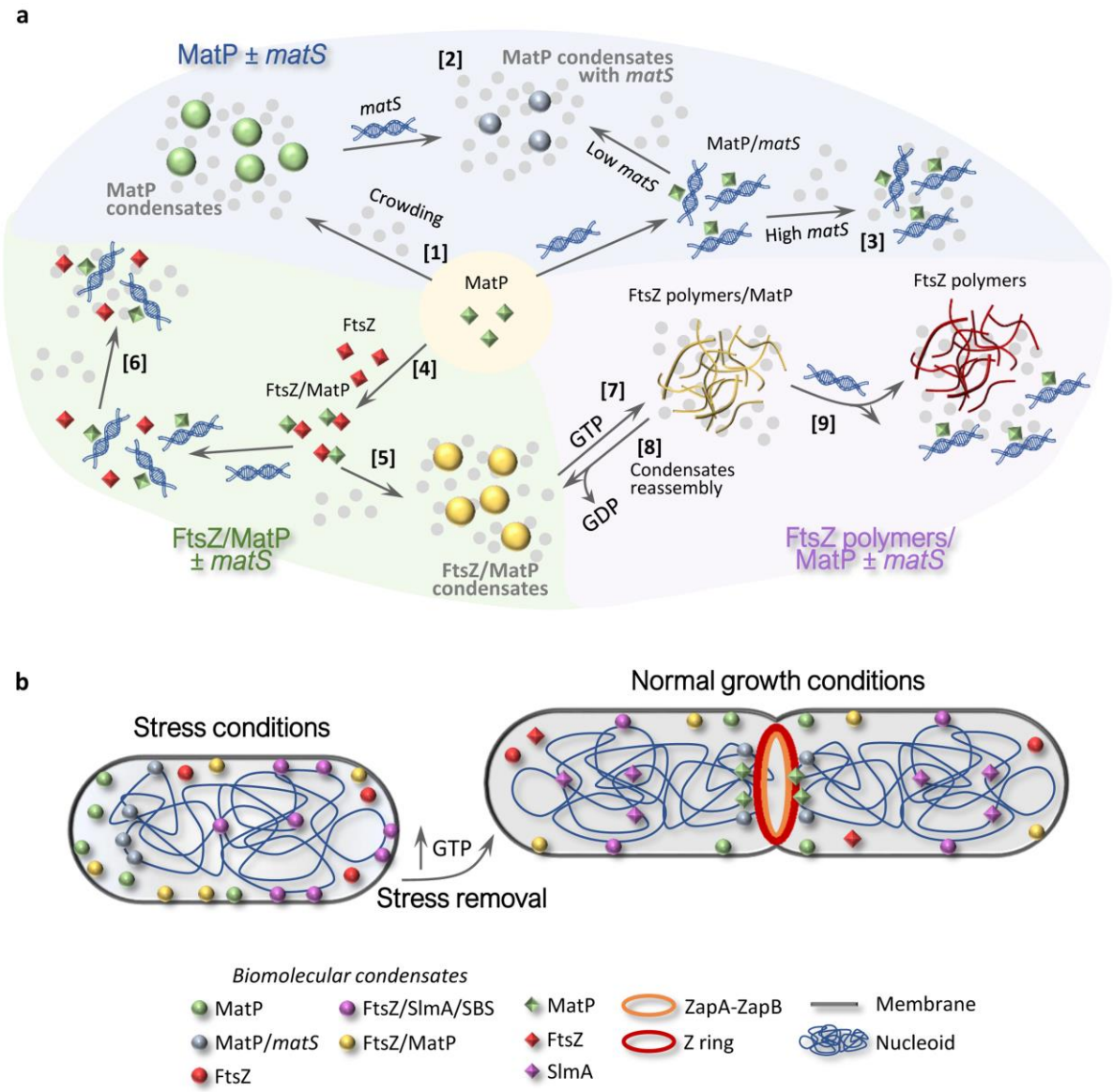

Figure 9. Schematic representation of the assembly and regulation of MatP biomolecular condensates and potential role of division proteins condensates under stress conditions. (**a**) In crowding conditions, MatP forms dynamic biomolecular condensates [1] where *matS* can incorporate [2], although the presence of high *matS* concentration prior to condensation precludes phase separation [3]. MatP interacts with FtsZ [4], forming crowding-driven heterotypic condensates [5], and *matS* disrupts the FtsZ/MatP complexes hindering condensation [6]. In the presence of GTP, FtsZ/MatP condensates evolve towards FtsZ polymers to which MatP is bound [7], and GTP depletion results in condensates reassembly

[8]. *matS* dissociates MatP from the FtsZ polymers [9]. (**b**) Biomolecular condensation of proteins involved in cell division may provide resistance to stress, as part of the mechanisms underlying development of persister cells. Under these conditions, MatP could be transiently stored within these compartments, with or without FtsZ, preferentially at the membrane. Incorporation of chromosomal *matS* into MatP condensates might contribute to nucleoid compaction (a known role of MatP (47)), possibly conferring resistance by halting cell cycle, as described for other NAPs (48). Reduced GTP levels in dormant cells (17, 18) would favor FtsZ homotypic and heterotypic condensates (with MatP, or with the nucleoid occlusion factor SlmA and its target DNA, SBS) that would keep the protein outside the division ring. GTP increase, upon stress release, would trigger assembly of FtsZ within the condensates into polymers (14–16), and those arising from FtsZ/MatP condensates would contain MatP, which would be dissociated from them by *matS*. Polymers elicited from FtsZ/SlmA/SBS condensates would be rapidly disassembled by the antagonist back to condensates (15), an effect counteracted by the division ring formation agonist ZapA (16). Under normal growth conditions, condensates would be found to a different extent; at division, some may remain assembled to store the large amount of FtsZ outside the division ring (46, 49); at stages other than division, condensates would store the whole FtsZ pool. MatP condensates enriched in *matS* could facilitate its role in Ter macrodomain compaction, while, at the membrane, they could serve to sequester MatP from the chromosome to allow binding of other proteins when required.

The formation of biomolecular condensates by MatP is probably driven by multivalency, a key determinant of protein phase separation, since structural analysis of this protein discards (at least when in complex with *matS*) the presence of the other feature usually associated, large unstructured regions (1). MatP contains multiple binding domains, including a central ribbon-helix-helix region that mediates the formation of MatP dimers and interacts with *matS* sites; an N-terminal four-helix bundle that also interacts with DNA; and a C-terminal flexible coiled-coil domain important for protein-protein recognition (22, 23). Coiled-coil domains are among the protein folding motifs more prone to biomolecular condensation

and, according to recent coarse-grained molecular simulations, their presence suffices to support phase separation (50). Many prokaryotic and eukaryotic proteins containing coiled-coils have been shown to undergo phase separation, including the cell division protein PodJ from *C. crescentus* (51), centrosomal proteins, transcription factors and RNA binding proteins ((50) and references therein). More studies will be required to ascertain the role of the coiled-coils and other structural elements in MatP condensation.

MatP membraneless compartments arising from phase separation are consistent with the originally described uneven cellular distribution pattern of this protein in bacteria (20). MatP accumulates at specific locations depending on the cell cycle stage, forming discrete foci that shift from the new pole to the cell center, ultimately splitting into two sister foci that remain juxtaposed until they move away from midcell. MatP foci were subsequently observed in other *in vivo* studies, and their number and distribution analyzed under different conditions (22, 23, 29, 52, 53). The dynamic and reversible nature of the MatP biomolecular condensates demonstrated in this study and the refined control of their assembly by *matS* could potentially explain how the MatP pool rapidly mobilizes and reorganizes within the cell during the course of the cell cycle.

Formation of condensates by MatP would also be favored by macromolecular crowding in the vicinity of the chromosome, which is coated by a high density of nucleoid associated proteins (NAPs), covering ~ 30% of the chromosome in the case of *E. coli* (54). Indeed, crowding-driven phase separation of NAPs such as histone-like heat-unstable nucleoid protein (HU), DNA-binding protein from starved cells (Dps), single-stranded DNA binding protein (SSB) and RNA polymerase (RNAP) (48, 55–57) has been reported. Interestingly, some of these proteins are involved in DNA compaction, including MatP, which is known to constrain the Ter macrodomain (47). It is possible that MatP biomolecular condensates allowing subsequent incorporation of *matS* sequences, or even assembled alongside low *matS* concentrations, could aid in DNA structural arrangement by this protein (Figure 9b).

Our results show a direct interaction between MatP and FtsZ that strongly promotes biomolecular condensation in crowded media into compartments (Figure 9). These compartments could be regarded as coacervates formed by a positively charged protein (MatP, pI 9.5) and a negatively charged protein (FtsZ, pI 4.6), consistent with the strong

dependence on ionic strength observed. FtsZ/MatP heterocomplexes were also detected in dilute conditions, including large complexes that could potentially represent incipient FtsZ/MatP biomolecular condensates, efficiently disrupted by *matS*.

FtsZ/MatP interaction may not play a role in the canonical positioning of the Z ring by the Ter linkage that involves also ZapA and ZapB (24) but, through the associated condensates, it could provide a means to store both proteins. FtsZ might be transiently pooled during cell cycle stages other than division, but possibly even at the moment of division to accommodate the ~ 60% of cellular FtsZ that is not in the Z ring (46, 49). In the case of MatP, its removal from the chromosome and accumulation at the membrane have been proposed to facilitate the function of proteins that help segregate the Ter region, like FtsK (29), and perhaps Topoisomerase IV (27).

We also propose that in response to certain signals in *E. coli* cells, MatP and FtsZ stored within the condensate reservoirs, located principally at the membrane according to our experiments in cell-like systems, could be easily mobilized. Condensates containing solely MatP would be detached from the membrane upon incorporation of *matS,* and high specific DNA concentrations that might locally arise would antagonize their assembly. Besides the negative regulation by *matS,* FtsZ/MatP condensates are also susceptible to disassembly by GTP, which would trigger the assembly of FtsZ polymers decorated by MatP, ultimately removed from them by *matS* (Figure 9a). The presence of FtsZ in MatP condensates provides this additional disassembly pathway involving GTP that facilitates dissociation of preformed condensates, which are more resistant to the action of *matS* according to our data. It remains to be determined whether FtsZ/MatP dissociation is required for canonical interaction of each protein with ZapA and ZapB, respectively, or if the FtsZ/MatP interaction itself is part of the Ter-linkage.

The interplay between MatP biomolecular condensates, *matS* DNA sequences, the membrane and other interacting molecules found here is strikingly reminiscent of how condensates regulate the activity of SSB protein, which is important for bacterial chromosome replication and maintenance (56). By analogy with MatP/*matS*, DNA accumulates in SSB compartments when at low concentrations relative to those of the protein, and inhibits phase separation at higher DNA:protein ratios. As with MatP, SSB foci

assemble at the membrane, which is explained by specific membrane-protein interaction. SSB condensates have been proposed to serve as a means to store SSB alongside interacting molecules, allowing rapid mobilization when required to repair damaged DNA. Reduction of condensation by nucleic acids has also been described for other systems, some of them involved in stress sensing. Examples are the stress granule proteins Pub1 and Pab1, whose phase separation is inhibited by RNA (58, 59).

Biomolecular condensates assembled in bacteria such as aggresomes, bacterial ribonucleoprotein bodies, polyP granules, condensates of the SSB, Dps or HU NAPs, among others, have been connected to dormant and persister cell states known to withstand threatening conditions (5). Condensates of Dps and HU confer protection through DNA compaction (48, 55), and this could also be the case of MatP phase separation, given the well-known role of this protein as a compactor of the Ter macrodomain (47). Additionally, a hallmark of these quiescent states is reversible arrest of cell growth and division (60). For this purpose, storage of cytokinesis factors and regulators like MatP and FtsZ inside DNA- and GTP-responsive compartments may be an effective strategy (Figure 9b), as previously proposed for FtsZ and FtsZ/SlmA condensates (14, 15).

Interestingly, the *E. coli* bacterial cell division condensates identified so far appear to be subjected to a regulation scheme in which DNA sequences act differently depending on whether the protein in the condensate enhances or inhibits Z ring assembly. Thus, DNA binding strongly promotes condensation of FtsZ with SlmA, a negative regulator of Z ring formation (15), consistent with an increase in multivalency by the DNA activation of SlmA. This gives rise to condensates in which FtsZ is sequestered along with its inhibitor ensuring efficient blockage of its assembly into the Z ring, even in the presence of agonists like ZapA (16). Such behavior would be predicted in quiescent or dormant cells. In contrast, depending on the local concentration, *matS* binding is detrimental for condensate formation by MatP, either on its own or with FtsZ. Moreover, incorporation of *matS* into MatP condensates dislodges them from the preferred protein storage location at the membrane, perhaps facilitating Ter linkage assembly and hence Z ring positioning at the cell center for normal cytokinesis, which should not occur in quiescent states.

Besides target DNA sequences, the other key player in the regulation of FtsZ-containing condensates is GTP, which is strongly depleted in quiescent states (17, 18) favoring the condensation-prone oligomeric forms of the protein (Figure 9b). GTP dissociates both the FtsZ/SlmA/DNA and the FtsZ/MatP condensates, although in the latter case *matS* is instrumental to obtain MatP-free FtsZ polymers and MatP/*matS* complexes available for interaction with ZapA, ZapB and other partners to resume cytokinesis upon release from stress (Figure 9). This reinforces the idea that biomolecular condensates containing bacterial cell division proteins could be involved in the development of persisters and, hence, could be regarded as new targets for molecules that can kill pernicious bacteria (61).

DATA AVAILABILITY

All data are available from the corresponding authors upon request.

SUPPLEMENTARY DATA

Supplementary Data are available at NAR online.

AUTHOR CONTRIBUTIONS

Inés Barros-Medina: investigation, formal analysis, visualization and writing— review and editing. Miguel Ángel Robles-Ramos: data curation, formal analysis, visualization, investigation and writing—review and editing. Marta Sobrinos-Sanguino: formal analysis, investigation and writing— review and editing. Juan Román Luque-Ortega: formal analysis and investigation. Carlos Alfonso: formal analysis and investigation. William Margolin: validation, funding acquisition, writing-review and editing. Germán Rivas: validation, funding acquisition, writing-review and editing. Begoña Monterroso: conceptualization, data curation, formal analysis, project administration, supervision, validation, writing—original draft, writing—review and editing. Silvia Zorrilla: conceptualization, data curation, formal analysis, funding acquisition, project administration, supervision, validation, writing—original draft and writing—review and editing. All authors gave final approval for publication and agreed to be held accountable for the work performed therein.

ACKNOWLEDGEMENTS

We thank the staff of CIB Margarita Salas Confocal Laser and Multidimensional Microscopy (M.T. Seisdedos and G. Elvira) and Molecular Interactions (Ó. Nuero) Facilities for excellent technical assistance, and the Technical Support Facility for invaluable input. We also thank Drs. V. Buschmann and E. Sisamakis for generous technical help with the time-resolved confocal instrument, M. Schumacher (Duke University) for kindly providing the MatP plasmid, and W. T. S. Huck and A. Piruska (Radboud University) for the kind gift of silicon masters with the chip designs.

FUNDING

This work was supported by Grant PID2019-104544GB-I00 funded by MICIU/AEI/10.13039/501100011033 and by Grant PID2022-136951NB-I00 funded by MICIU/AEI/10.13039/501100011033 and by ERDF, EU. W.M. was supported by National Institutes of Health grant GM131705. I.B.-M. was supported by Grant FPU2020-05620 funded by MICIU/AEI/10.13039/501100011033 and by ESF Investing in your future. M.A.R.-R. was supported by Grant BES-2017-082003 funded by MICIU/AEI/10.13039/501100011033 and by ESF Investing in your future. M.S.-S. was supported by Grant PTA2020-018219-I funded by MICIU/AEI/10.13039/501100011033. The Systems Biochemistry of Bacterial Division group (CIB Margarita Salas) participates in the CSIC Conexiones LifeHUB (PIE-202120E047). The funders had no role in study design, data collection and interpretation, or the decision to submit the work for publication.

CONFLICT OF INTEREST

We declare we have no competing interests.

REFERENCES

1. Banani,S.F., Lee,H.O., Hyman,A.A. and Rosen,M.K. (2017) Biomolecular condensates: organizers of cellular biochemistry. Nature reviews. Molecular cell biology, 18, 285–298.

2. Shin,Y. and Brangwynne,C.P. (2017) Liquid phase condensation in cell physiology and disease. Science, 357.

3. Alberti,S. and Dormann,D. (2019) Liquid-Liquid Phase Separation in Disease. Annual review of genetics, 53, 171–194.

4. Azaldegui,C.A., Vecchiarelli,A.G. and Biteen,J.S. (2020) The emergence of phase separation as an organizing principle in bacteria. Biophysical journal, 119, 1–16.

5. Monterroso,B., Margolin,W., Boersma,A.J., Rivas,G., Poolman,B. and Zorrilla,S. (2024) Macromolecular Crowding, Phase Separation, and Homeostasis in the Orchestration of Bacterial Cellular Functions. Chem. Rev., 124, 1899–1949.

6. Ditlev,J.A., Case,L.B. and Rosen,M.K. (2018) Who's In and Who's Out—Compositional Control of Biomolecular Condensates. Journal of Molecular Biology, 430, 4666–4684.

7. Fare,C.M., Villani,A., Drake,L.E. and Shorter,J. (2021) Higher-order organization of biomolecular condensates. Open Biol., 11, 210137.

8. Lasker,K., Boeynaems,S., Lam,V., Scholl,D., Stainton,E., Briner,A., Jacquemyn,M., Daelemans,D., Deniz,A., Villa,E., et al. (2022) The material properties of a bacterial-derived biomolecular condensate tune biological function in natural and synthetic systems. Nat Commun, 13, 5643.

9. Alberti,S., Gladfelter,A. and Mittag,T. (2019) Considerations and Challenges in Studying Liquid-Liquid Phase Separation and Biomolecular Condensates. Cell, 176, 419–434.

10. Jin,X., Lee,J.-E., Schaefer,C., Luo,X., Wollman,A.J.M., Payne-Dwyer,A.L., Tian,T., Zhang,X., Chen,X., Li,Y., et al. (2021) Membraneless organelles formed by liquid-liquid phase separation increase bacterial fitness. Sci. Adv., 7, eabh2929.

11. Cameron,T.A. and Margolin,W. (2023) Insights into the assembly and regulation of the bacterial divisome. Nat Rev Microbiol, 10.1038/s41579-023-00942-x.

12. Schumacher,M.A. (2017) Bacterial Nucleoid Occlusion: Multiple Mechanisms for Preventing Chromosome Bisection During Cell Division. Sub-cellular biochemistry, 84, 267–298.

13. Bailey,M.W., Bisicchia,P., Warren,B.T., Sherratt,D.J. and Männik,J. (2014) Evidence for Divisome Localization Mechanisms Independent of the Min System and SlmA in Escherichia coli. PLoS Genet, 10, e1004504.

14. Robles-Ramos,M.A., Zorrilla,S., Alfonso,C., Margolin,W., Rivas,G. and Monterroso,B. (2021) Assembly of bacterial cell division protein FtsZ into dynamic biomolecular condensates. Biochimica et biophysica acta. Molecular cell research, 1868, 118986.

15. Monterroso,B., Zorrilla,S., Sobrinos-Sanguino,M., Robles-Ramos,M.A., Lopez-Alvarez,M., Margolin,W., Keating,C.D. and Rivas,G. (2019) Bacterial FtsZ protein forms phase-separated condensates with its nucleoid-associated inhibitor SlmA. EMBO reports, 20, e45946.

16. Monterroso,B., Robles-Ramos,M.Á., Sobrinos-Sanguino,M., Luque-Ortega,J.R., Alfonso,C., Margolin,W., Rivas,G. and Zorrilla,S. (2023) Bacterial division ring stabilizing ZapA versus destabilizing SlmA modulate FtsZ switching between biomolecular condensates and polymers. Open Biol., 13, 220324.

17. Harms,A., Maisonneuve,E. and Gerdes,K. (2016) Mechanisms of bacterial persistence during stress and antibiotic exposure. Science, 354.

18. Zhang,Y., Zbornikova,E., Rejman,D. and Gerdes,K. (2018) Novel (p)ppGpp Binding and Metabolizing Proteins of Escherichia coli. mBio, 9.

19. Yu,J., Liu,Y., Yin,H. and Chang,Z. (2019) Regrowth-delay body as a bacterial subcellular structure marking multidrug-tolerant persisters. Cell discovery, 5, 8.

20. Mercier,R., Petit,M.-A., Schbath,S., Robin,S., El Karoui,M., Boccard,F. and Espéli,O. (2008) The MatP/matS Site-Specific System Organizes the Terminus Region of the E. coli Chromosome into a Macrodomain. Cell, 135, 475–485.

21. Seba,M., Boccard,F. and Duigou,S. (2024) Activity of MukBEF for chromosome management in E. coli and its inhibition by MatP. 10.7554/eLife.91185.2.

22. Dupaigne,P., Tonthat,N.K., Espéli,O., Whitfill,T., Boccard,F. and Schumacher,M.A. (2012) Molecular Basis for a Protein-Mediated DNA-Bridging Mechanism that Functions in Condensation of the E. coli Chromosome. Molecular Cell, 48, 560–571.

23. Espéli,O., Borne,R., Dupaigne,P., Thiel,A., Gigant,E., Mercier,R. and Boccard,F. (2012) A MatP-divisome interaction coordinates chromosome segregation with cell division in E. coli: Chromosome-divisome interplay. The EMBO Journal, 31, 3198–3211.

24. Mannik,J. and Bailey,M.W. (2015) Spatial coordination between chromosomes and cell division proteins in Escherichia coli. Frontiers in microbiology, 6, 306.

25. Ortiz,C., Natale,P., Cueto,L. and Vicente,M. (2016) The keepers of the ring: regulators of FtsZ assembly. FEMS microbiology reviews, 40, 57–67.

26. Pazos,M., Natale,P., Margolin,W. and Vicente,M. (2013) Interactions among the early E scherichia coli divisome proteins revealed by bimolecular fluorescence complementation. Environmental Microbiology, 15, 3282–3291.

27. Nolivos,S., Upton,A.L., Badrinarayanan,A., Müller,J., Zawadzka,K., Wiktor,J., Gill,A., Arciszewska,L., Nicolas,E. and Sherratt,D. (2016) MatP regulates the coordinated action of topoisomerase IV and MukBEF in chromosome segregation. Nat Commun, 7, 10466.

28. Fisher,G.L., Bolla,J.R., Rajasekar,K.V., Mäkelä,J., Baker,R., Zhou,M., Prince,J.P., Stracy,M., Robinson,C.V., Arciszewska,L.K., et al. (2021) Competitive binding of MatP and topoisomerase IV to the MukB hinge domain. Elife, 10, e70444.

29. Monterroso,B., Zorrilla,S., Sobrinos-Sanguino,M., Robles-Ramos,M.Á., Alfonso,C., Söderström,B., Meiresonne,N.Y., Verheul,J., Den Blaauwen,T. and Rivas,G. (2019) The Bacterial DNA Binding Protein MatP Involved in Linking the Nucleoid Terminal Domain to the Divisome at Midcell Interacts with Lipid Membranes. mBio, 10, e00376-19.

30. Rivas,G., López,A., Mingorance,J., Ferrándiz,M.J., Zorrilla,S., Minton,A.P., Vicente,M. and Andreu,J.M. (2000) Magnesium-induced linear self-association of the FtsZ bacterial cell division protein monomer. The primary steps for FtsZ assembly. J Biol Chem, 275, 11740–9.

31. Reija,B., Monterroso,B., Jimenez,M., Vicente,M., Rivas,G. and Zorrilla,S. (2011) Development of a homogeneous fluorescence anisotropy assay to monitor and measure FtsZ assembly in solution. Anal Biochem, 418, 89–96.

32. Monterroso,B., Zorrilla,S., Sobrinos-Sanguino,M., Keating,C.D. and Rivas,G. (2016) Microenvironments created by liquid-liquid phase transition control the dynamic distribution of bacterial division FtsZ protein. Scientific reports, 6, 35140.

33. Wang,J., Choi,J.-M., Holehouse,A.S., Lee,H.O., Zhang,X., Jahnel,M., Maharana,S., Lemaitre,R., Pozniakovsky,A., Drechsel,D., et al. (2018) A Molecular Grammar Governing the Driving Forces for Phase Separation of Prion-like RNA Binding Proteins. Cell, 174, 688-699.e16.

34. Mellouli,S., Monterroso,B., Vutukuri,H.R., te Brinke,E., Chokkalingam,V., Rivas,G. and Huck,W.T.S. (2013) Self-organization of the bacterial cell-division protein FtsZ in confined environments. Soft Matter, 9, 10493–10500.

35. Schneider,C.A., Rasband,W.S. and Eliceiri,K.W. (2012) NIH Image to ImageJ: 25 years of image analysis. Nat Methods, 9, 671–675.

36. Small,E. and Addinall,S.G. (2003) Dynamic FtsZ polymerization is sensitive to the GTP to GDP ratio and can be maintained at steady state using a GTP-regeneration system. Microbiology, 149, 2235–2242.

37. Skakun,V.V., Hink,M.A., Digris,A.V., Engel,R., Novikov,E.G., Apanasovich,V.V. and Visser,A.J.W.G. (2005) Global analysis of fluorescence fluctuation data. Eur Biophys J, 34, 323–334.

38. Schuck,P. (2000) Size-distribution analysis of macromolecules by sedimentation velocity ultracentrifugation and lamm equation modeling. Biophysical journal, 78, 1606–19.

39. Schuck,P. (2003) On the analysis of protein self-association by sedimentation velocity analytical ultracentrifugation. Analytical Biochemistry, 320, 104–124.

40. Balbo,A., Minor,K.H., Velikovsky,C.A., Mariuzza,R.A., Peterson,C.B. and Schuck,P. (2005) Studying multiprotein complexes by multisignal sedimentation velocity analytical ultracentrifugation. Proc. Natl. Acad. Sci. U.S.A., 102, 81–86.

41. Royer,C.A., Smith,W.R. and Beechem,J.M. (1990) Analysis of binding in macromolecular complexes: A generalized numerical approach. Analytical Biochemistry, 191, 287–294.

42. Rosales,T. and Royer,C.A. (2008) A graphical user interface for BIOEQS: A program for simulating and analyzing complex biomolecular interactions. Analytical Biochemistry, 381, 270–272.

43. Chen,H., Ahsan,S.S., Santiago-Berrios,M.B., Abruña,H.D. and Webb,W.W. (2010) Mechanisms of Quenching of Alexa Fluorophores by Natural Amino Acids. J. Am. Chem. Soc., 132, 7244–7245.

44. Monterroso,B., Ahijado-Guzman,R., Reija,B., Alfonso,C., Zorrilla,S., Minton,A.P. and Rivas,G. (2012) Mg(2+)-linked self-assembly of FtsZ in the presence of GTP or a GTP analogue involves the concerted formation of a narrow size distribution of oligomeric species. Biochemistry, 51, 4541–50.

45. Ahijado-Guzman,R., Alfonso,C., Reija,B., Salvarelli,E., Mingorance,J., Zorrilla,S., Monterroso,B. and Rivas,G. (2013) Control by potassium of the size distribution of Escherichia coli FtsZ polymers is independent of GTPase activity. The Journal of biological chemistry, 288, 27358–65.

46. Erickson,H.P., Anderson,D.E. and Osawa,M. (2010) FtsZ in bacterial cytokinesis: cytoskeleton and force generator all in one. Microbiol Mol Biol Rev, 74, 504–28.

47. Thiel,A., Valens,M., Vallet-Gely,I., Espéli,O. and Boccard,F. (2012) Long-range chromosome organization in E. coli: a site-specific system isolates the Ter macrodomain. PLoS Genet, 8, e1002672.

48. Janissen,R., Arens,M.M.A., Vtyurina,N.N., Rivai,Z., Sunday,N.D., Eslami-Mossallam,B., Gritsenko,A.A., Laan,L., de Ridder,D., Artsimovitch,I., et al. (2018) Global DNA Compaction in Stationary-Phase Bacteria Does Not Affect Transcription. Cell, 174, 1188-1199 e14.

49. Margolin,W. (2020) Bacterial Division: Journey to the Center of the Cell. Current Biology, 30, R114–R116.

50. Ramirez,D.A., Hough,L.E. and Shirts,M.R. (2024) Coiled-coil domains are sufficient to drive liquid-liquid phase separation in protein models. Biophysical Journal, 123, 703–717.

51. Tan,W., Cheng,S., Li,Y., Li,X.-Y., Lu,N., Sun,J., Tang,G., Yang,Y., Cai,K., Li,X., et al. (2022) Phase separation modulates the assembly and dynamics of a polarity-related scaffold-signaling hub. Nat Commun, 13, 7181.

52. Männik,J., Castillo,D.E., Yang,D., Siopsis,G. and Männik,J. (2016) The role of MatP, ZapA and ZapB in chromosomal organization and dynamics in Escherichia coli. Nucleic Acids Res, 44, 1216–1226.

53. Sadhir,I. and Murray,S.M. (2023) Mid-cell migration of the chromosomal terminus is coupled to origin segregation in Escherichia coli. Nat Commun, 14, 7489.

54. Finkelstein,I.J. and Greene,E.C. (2013) Molecular traffic jams on DNA. Annu Rev Biophys, 42, 241–263.

55. Gupta,A., Joshi,A., Arora,K., Mukhopadhyay,S. and Guptasarma,P. (2023) The bacterial nucleoid-associated proteins, HU and Dps, condense DNA into context-dependent biphasic or multiphasic complex coacervates. Journal of Biological Chemistry, 299, 104637.

56. Harami,G.M., Kovács,Z.J., Pancsa,R., Pálinkás,J., Baráth,V., Tárnok,K., Málnási-Csizmadia,A. and Kovács,M. (2020) Phase separation by ssDNA binding protein controlled via protein−protein and protein−DNA interactions. Proc. Natl. Acad. Sci. U.S.A., 117, 26206–26217.

57. Ladouceur,A.M., Parmar,B.S., Biedzinski,S., Wall,J., Tope,S.G., Cohn,D., Kim,A., Soubry,N., Reyes-Lamothe,R. and Weber,S.C. (2020) Clusters of bacterial RNA polymerase are biomolecular condensates that assemble through liquid-liquid phase separation. Proceedings of the National Academy of Sciences of the United States of America, 117, 18540–18549.

58. Kroschwald,S., Munder,M.C., Maharana,S., Franzmann,T.M., Richter,D., Ruer,M., Hyman,A.A. and Alberti,S. (2018) Different Material States of Pub1 Condensates Define Distinct Modes of Stress Adaptation and Recovery. Cell reports, 23, 3327–3339.

59. Riback,J.A., Katanski,C.D., Kear-Scott,J.L., Pilipenko,E.V., Rojek,A.E., Sosnick,T.R. and Drummond,D.A. (2017) Stress-Triggered Phase Separation Is an Adaptive, Evolutionarily Tuned Response. Cell, 168, 1028-1040 e19.

60. Fisher,R.A., Gollan,B. and Helaine,S. (2017) Persistent bacterial infections and persister cells. Nature reviews. Microbiology, 15, 453–464.

61. Zorrilla,S., Monterroso,B., Robles-Ramos,M.-Á., Margolin,W. and Rivas,G. (2021) FtsZ Interactions and Biomolecular Condensates as Potential Targets for New Antibiotics. Antibiotics, 10, 254.